AN EXPERIMENTAL INVESTIGATION OF ICEPHOBICITY AND HYDROPHOBICITY OF CONCRETE SURFACE TREATED WITH PAVIX

by:

Hussein Hashemi Senejani

Presented to the Faculty of the Graduate School of
The University of Texas at Arlington
In Partial Fulfillment of the Requirements for the Degree of

MASTER OF SCIENCE IN CIVIL ENGINEERING

The University of Texas at Arlington

Department of Civil Engineering

August 2022

Abstract

AN EXPERIMENTAL INVESTIGATION OF ICEPHOBICITY AND HYDROPHOBICITY OF CONCRETE SURFACE TREATED WITH PAVIX

Hussein Hashemi Senejani

The University of Texas at Arlington, 2022

Supervising Professor: Dr. Xinbao Yu

High ice adhesion is a significant problem in several industries. The majority of practical issues brought on by ice adhesion are still not fully resolved, and the ice-adhesion mechanism is still poorly understood. Ice adhesion is a complex phenomenon that becomes more intricate when salt is involved, as in many marine cases. Reducing ice adhesion by generating hydrophobic surfaces might be advantageous in many applications as a passive ice removal strategy. Lowering adhesion may reduce friction, abrasion, and damage to structures in a maritime environment, as well as any surface prone to ice development. This process may also be utilized as a more environmentally friendly road deicing procedure. To estimate the effects of a topical treatment on shear adhesion of ice on concrete surfaces, a series of direct shear tests were performed on concrete treated with

a waterproofing product named PAVIX. Chem-Crete PAVIX is a multi-crystallization enhancer, a patented, dual-crystalline engineered waterproofing technology. TxDOT standard Class S concrete is used as control concrete and mixed at two water-cement ratios, 0.45 and 0.43. Ice-adhesion shear tests were performed on control and PAVIX-treated concrete disks using a customized direct shear test device at two controlled sub-freezing temperatures, 30 ºF and 13 ºF. In addition, thermal conductivity was measured using a KD2 RK-1 heat probe. Specific heat capacity was measured using a custom-made calorimetric box. Water repellent property and contact angle were measured using a tensiometer under static and receding conditions. Results show an excellent reduction of ice-adhesion for PAVIX-treated concrete combined with surface hydrophobicity. The measured results quantify the anti-icing benefit of PAVIX treatment and provide insights into understanding the anti-icing mechanism of the treated concrete. Further investigations must follow to establish a standard for the testing methods used. With increased tests and variations in the test plan, the ice concrete adhesion would be better understood.

Keywords: Concrete; Ice adhesion; Shear strength; Pavement deicing

Acknowledgments

I would like to express my gratitude to Dr. Xinbao Yu, my academic advisor and supervisor for giving me the opportunity to work on this project and entrusting me with its responsibilities. I am also truly thankful to the members of my graduate committee, Dr. Warda Ashraf and Dr. Azijul Islam for their time and insights for this project. I would like to thank my colleagues Mehran Azizian who helped me with running the main tests of this project, Gang Lei, Omid and many others who helped with all the research work throughout my stay at UTA. The financial support from International Chem-Crete company is highly appreciated for this research work.

My deepest gratitude goes to my family and their warmth and support throughout this period. I was thousands of miles away from home, living on my own for the first time and without them I could not stand the tests of time. I hope that one day I could return their kindness.

August 10th 2022

Table Of Contents

List Of Figures

List Of Tables

Chapter 1 Introduction

1.1 Overview

In many industries, including transportation, aviation, and power transmission, ice adhesion has been an issue causing hazardous or economic problems (Chen et al. 2018b; Gustafson 1982; Palacios et al. 2012). To mitigate such problems, decreasing ice adhesion strength is one of the most well received approaches to make anti-icing surfaces (Hejazi et al. 2013; Kreder et al. 2016; Lv et al. 2014). This would make ice removal a needed practice for preventing many unsafe conditions (Lv et al. 2014; Mittal 2012) and protecting infrastructure from icing an easier task (Makkonen 1998; Makkonen et al. 2001; Makkonen 2012). Implementing this reduction method requires a comprehensive understanding of ice adhesion mechanisms (Rønneberg et al. 2019), but the fundamental physics of ice adhesion requires more investigation (Petrenko V. F. 2006).

Among various deicing methods, three main approaches are using chemicals, heating, or creating hydrophobic (the physical property that repels material from water) surfaces. Despite the high efficiency of chemicals like chloride-based deicers (Shi et al. 2010), they may result in drastic environmental and even some structural damages (Fay and Shi 2012; Shi et al. 2010). A more environmental friendly approach for pavement passive deicing could be achieved using ice adhesion theory of hydrophobic surfaces (Chen et al. 2018a). Thus, the passive method of creating a hydrophobic surface to reduce ice bonding is becoming a popular option to explore in research (Ma 2014; Yang et al. 2011).

Among pavement types, cement concrete pavements are more hydrophilic in comparison with asphalt mixtures, making their ice adhesion strength higher, thus increasing the practical interest of reduction of its ice bonding (Chen et al. 2018a). There have been some previous attempts of

hydrophobic cement concrete, This includes usage of nanotechnology in cement concrete (Sanchez and Sobolev 2010; Sobolev 2016), with goals of hydrophobic surface development. The effectiveness of treatment of concrete pavements is also highly dependent on the type of concrete pavements. For instance, concrete pavements made up of pervious concrete are highly permeable (Joshaghani et al. 2014) and the hydrophobic material can easily pass through the pores.

There are a number of existing methods to measure ice adhesion strength used in the past (Kasaai M. R. 2004; Makkonen 2012; Schulz and Sinapius 2015). The tests include field and laboratory studies, however, there are no testing standards available and testing methods vary for each research team (Schulz and Sinapius 2015; Wang et al. 2014). This lack of standardized testing techniques leads to a challenging cross-examination and comparison between research results (Barker et al. 2021; Fortin and Perron 2012; Javan-Mashmool et al. 2006; Schulz and Sinapius 2015). A review of test programs to measure ice adhesion on concrete by Barker et al. (Barker et al. 2021) and a review of ice-pavement adhesion by Chen et al. (Chen et al. 2018a) are two recent attempts to provide a bigger picture to address this lack of consistency in testing approaches.

The world is moving towards more sustainable technologies; specifically in civil engineering and geotechnical engineering, use of new technologies like energy piles, GSHPs, concrete admixtures or coating have been studies both experimentally (Hashemi Senejani et al. 2020) and numerically (Yazdani Cherati et al. 2020) and are of great research interest. An experimental investigation was therefore suggested to evaluate the performance of a potential sustainable solution to the icing problem. In this experimental investigation, direct shear tests were adopted to investigate the ice adhesion strength of freshwater ice formed on concrete surfaces with and without PAVIX treatment. Chem-Crete PAVIX CCC100, is a patented Dual-Crystalline, penetrating concrete and masonry sealer. It is a water-based and environmentally friendly waterproofing product that

combines hygroscopic and hydrophilic crystals for pore-blocking function and hydrophobic material for pore lining. The objectives of this research, therefore, could be described as the assessment of ice adhesion strength for PAVIX treated and controlled concrete specimens at two different temperatures and two water-to-cement (w/c) ratios. Additionally, the evaluation of the water contact angle (static and receding) of PAVIX-treated and control concrete specimens to better understand the hydrophobic characteristics of the treatment is conducted. Thermal conductivity and specific heat capacity of the control samples were also measured to better understand the relations between variables. The effects of the treatment and the possible involving mechanisms are then discussed. Even though the focus of the research is on pavement deicing, such remedies could be used in other infrastructure fields like abrasion reduction of concrete surfaces in cold regions.

1.2 Objectives

The objectives of this research study are:

1) Assessment of ice adhesion strength for PAVIX treated and control concrete specimens at two different temperatures and two water-to-cement (w/c) ratios.

2) Evaluation of the water contact angle (static and receding) of PAVIX-treated and control concrete specimens.

3) Determination of other thermal properties of concrete, thermal conductivity, and specific heat capacity

1.3 Problem Statement

Based on the review of previous research on ice adhesion, the majority of research to date has been on how ice adheres to different types of constructions, such as piles, lock walls, and dams. There

are many icing-related studies in existence. However, due to a lack of a standardized testing method and the variety of testing procedures, cross-comparison of study outcomes is difficult. There is the possibility of development for a standard testing method to measure the ice adhesion and trying new solution to reduce the adhesion like treatment for concrete surfaces like pavements. This study provides the initial step of an experimental investigation to measure ice adhesion on concrete under various variables. The performance of newly developed treatments for concrete can lead to the elimination of ice adhesion problems and the reduction of their costs. The details of the experiments are described in the upcoming chapters.

1.4 Thesis Outline

This study is described in 5 chapters. The first chapter provides the overview of the study, the objectives, and the rationale behind the study in the problem statement section. Chapter 2 provides a brief review of the prior work in ice concrete adhesion with an emphasis on laboratory and experimental setups and a brief description of the material used for topical treatment. Chapter 3 provides the details of the laboratory investigations performed including the different types of tests planned, the preparations of testing platforms and a sample result of each test type to better demonstrate the data collection procedure. Chapter 4 presents the results of the experiments and their analysis. Chapter 5 provides a summary of the endeavor and the conclusions of the study; the limitations of the study are discussed and recommendations for future continuation of this line of study is given. A list of references is included at the end of this study. Finally, the full results of laboratory tests with corresponding pictures of the specimens are included in appendix A.

Chapter 2 Literature Review

2.1 Introduction

In this chapter, a review of past studies regarding ice and concrete interactions will be provided. Ice creates many problems on concrete structures, specifically in cold regions, damages including abrasion caused by ice and the detrimental bonding of ice and concrete are of high research interest. Previous research, their methodologies, and their results are reviewed. Ice loads and interactions are critical considerations for maritime concrete structures such as bridges, light piers, dams, and wharves in colder climates. Material loss from the concrete surface is caused by continuous or intermittent ice impact or their relative motion. This activity may shorten the life of the structure, raise maintenance expenses, or cause major erosion damage during its lifetime (Saeki H. 2010).

2.2 Shear, Sliding, and Friction Laboratory Studies

Temperature, surface roughness, water salinity, etc., are among the parameters studied in previous research on the friction of ice. Saeki reported their observation that shear strength increase as temperature decreases (Saeki et al. 1985). Their team also investigated the friction coefficient variations of ice under various temperatures and parameters. Figure 2.1 shows the test schematics used. The friction test was conducted on sea ice against various construction materials including concrete, with varying surface roughness, temperature, shearing velocity and, in both submerged and dry conditions. Other effects of parameters like ice growth direction, normal stress and contact area were also investigated.

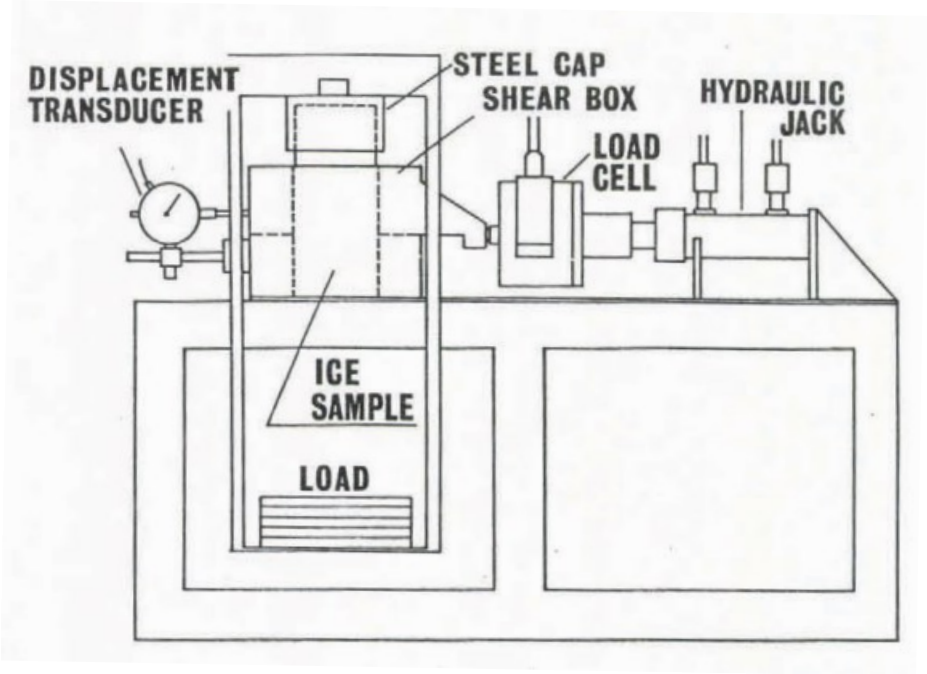

Figure 2.1 Schematics of direct shear test on ice (Saeki et al. 1985)

The experiment was carried out using a horizontal sliding frame linked to a hydraulic jack, on which an ice sample was put above the building material samples. During the test, the ice sample stayed stationary, while the construction material samples were moved. During the experiment, the ice temperature was the same as the air temperature. To hold the ice in place, a steel cap was utilized, and weights were put on top of the steel cap to generate steady vertical stress on the ice. The shearing velocity of the material samples was regulated by the hydraulic jack. The horizontal movement was introduced 10 seconds after the vertical force was imposed. A displacement transducer was mounted to the test platform to detect the relative velocity. A load cell affixed to the steel cap used to contain the ice was used to measure the friction force. The applied normal loading was determined by adding the applied weight and the steel cap weight. Figure 2.2 depicts the experiment's mechanism.

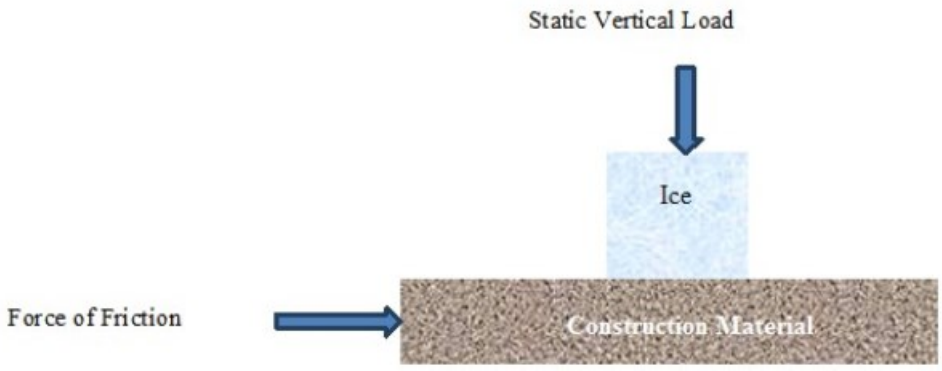

Figure 2.2 Mechanism of the laboratory experiment (H. Saeki, 1986)

The friction coefficient was shown to be temperature, surface roughness, and relative velocity dependent. The friction coefficient, like shear strength, rises with decreasing temperature, but kinetic friction decreases with higher normal stress. Because kinetic friction is greatly influenced by surface roughness, the test specimen surfaces were polished to cover the maximum surface area while avoiding roughness disparities. In another study, Kinetic friction coefficients between sea ice and various plastics, coatings, and metals were investigated utilizing normal stress up to 0.23 MPa. The ice friction coefficients for the majority of the test materials were found to fluctuate little with normal load (Huovinen S. 1990).

A further experiment assessed concrete abrasion caused by sea ice (Itoh Y. 1988).This effort adapted H. Saeki's prior experimental setup and tested sea ice and three different concrete mixtures. Their laboratory test setup can be seen in Figure 2.3.

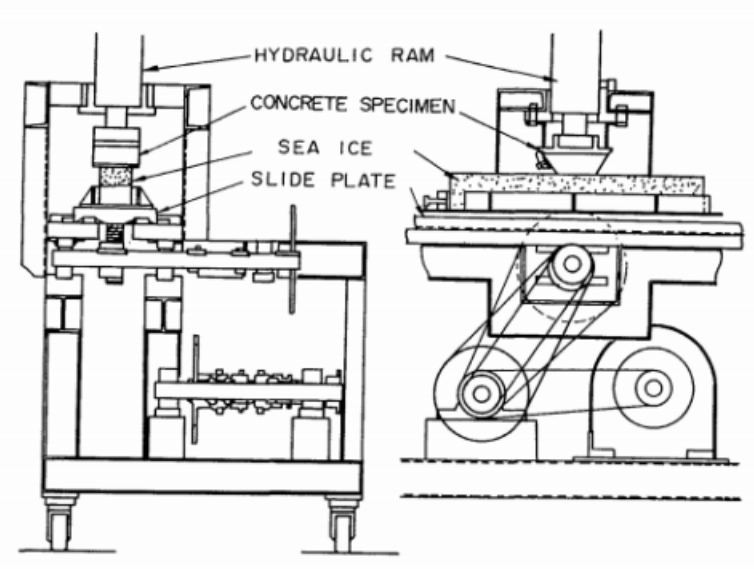

Figure 2.3 Apparatus and experiment setup (Itoh Y. 1988)

The concrete specimen was placed over an ice block so that the edges of the ice and concrete samples did not come into contact, since the widths of the concrete specimen and the ice block were 10 and 8 cm, respectively. The margins were utilized as a reference point for assessing concrete abrasion following the test. The sea ice on the sliding plate is 70x8 cm and is 5 or 10 cm thick. A hydraulic ram was used to apply variable contact pressure to the concrete sample over the ice sample. The sliding plate's reciprocating motion was utilized to assess both static and kinetic ice friction on the concrete sample. When the ice sample had been sufficiently abraded, the test was halted, and it was then restarted using a fresh piece of ice. The air temperature of the test room was constant, and the temperature of the ice specimen was recorded at each rest during the experiment. The concrete surface was measured before and after the experiment across the five traverse lines (Figure 2.4). The ablated ice could be removed from the interface using an air blower in this test setting. Since the air coming from the blower was the same temperature as the ice sample, the air also served to minimize frictional heat generated by the ice block surface.

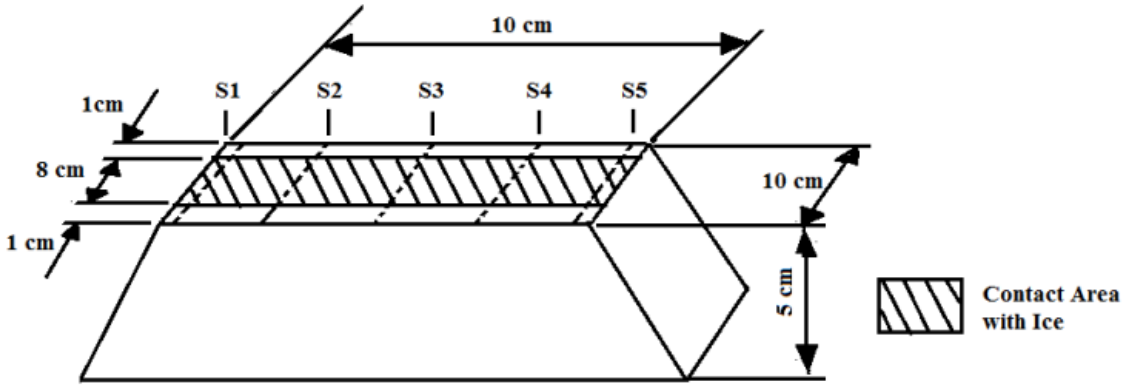

Figure 2.4 Traverse line and concrete specimen (Itoh Y. 1988)

Several ice and concrete specimens were utilized in this investigation. Ice samples had 35 percent saltiness and ranged in density from 0.90 to 0.92 grams per cubic meter. The aggregate and surface treatment have a significant impact on the strength, resilience, and abrasion of concrete. The concrete sample mixes were designed with various aggregates, including normal aggregate, lightweight coarse aggregate, and normal fine aggregate, as well as lightweight fine and coarse aggregate, which have corresponding strengths of 350, 568, and 700 kgf/cm respectively. Polyurethane resin lining, polymer impregnation, and resin mortar lining were applied as surface treatments. The experiment's variables were relative velocity (1, 5, 203 cm/sec), temperature (-5, -10, -20 °C), and contact pressure (5, 10, 15, 20, 30 kgf/cm^2). When the contact pressure rises, it is discovered that the concrete abrasion increases linearly for each ice temperature. The test could not be completed because the ice block started dissolving when the experiment was carried out at -5°C and -10°C and the contact pressure surpassed 20 kgf/cm. This is because the contact pressure was very relatively close to the ice block's crushing strength. It was discovered that the relative velocity, compressive strength, and aggregate type of concrete all had only a negligibly little impact on the rate of concrete wear. These results led to the recommendation of resin mortar lining

or polyurethane resin lining as a surface treatment to lessen concrete abrasion. As opposed to mortar enhancement techniques such steel fiber reinforcing or polymer impregnation, which were shown to be ineffectual as wear-reducing surface treatments, this lining lessens the friction between the structure and the sea ice.

In experiments done by Huovinen (1990), abrasion-resistant concrete mixtures were repeatedly frozen and thawed before being subjected to abrasion testing. Because the obtruded aggregate stones cause the fine concrete particles to abrade, the ice force was then measured in the lab against those aggregate stones. The concrete specimen was positioned on the bow of an icebreaker at waterline level for additional field tests to determine the concrete's wear rate in seawater (Huovinen S. 1990). Huovinen also outlined the mechanism of sea ice-induced concrete structure wear. Depending on the impact of the ice loading, the consequence of concrete abrasion may be physical, chemical, or mechanical. Due to fractures in the structure brought on by freezing water pressure and concrete shrinkage brought on by temperature changes, moisture and salt can physically harm the concrete. Sea ice contacts with the structure results in mechanical abrasion damage. Due to the resulting wear of the finer concrete components and exposure of the aggregate stones, more severe mechanical damage ensues.

Brief descriptions of the test equipment utilized at the Finnish VTT Technical Research Center are provided by Makkonen (2012). Their setup can be seen in Figure 2.5. The testing equipment is relevant even though tests on concrete were not conducted using it because of its parallels to existing test procedures for concrete and possible application for coming up with a standard test configuration. 30-mm diameter ice cylinders were bonded to aluminum substrate samples with dimensions of 100X100X10 mm at 10°C, starting from a liquid water condition, and after 24 hours of freezing. With a speed of 3.2X104 m/s, a belt drive was used to apply the shear force. The

exploration of coatings for deicing and anti-icing objectives was the study's primary goal, but it also created a theoretical model for calculating ice adhesion that was used to compare laboratory tests. Theoretical predictions and laboratory measurements, according to the author, both support the notion that materials having a broad water contact angle and the often accompanying low surface energy are likely to have poor adhesion strength with ice (Makkonen 2012).

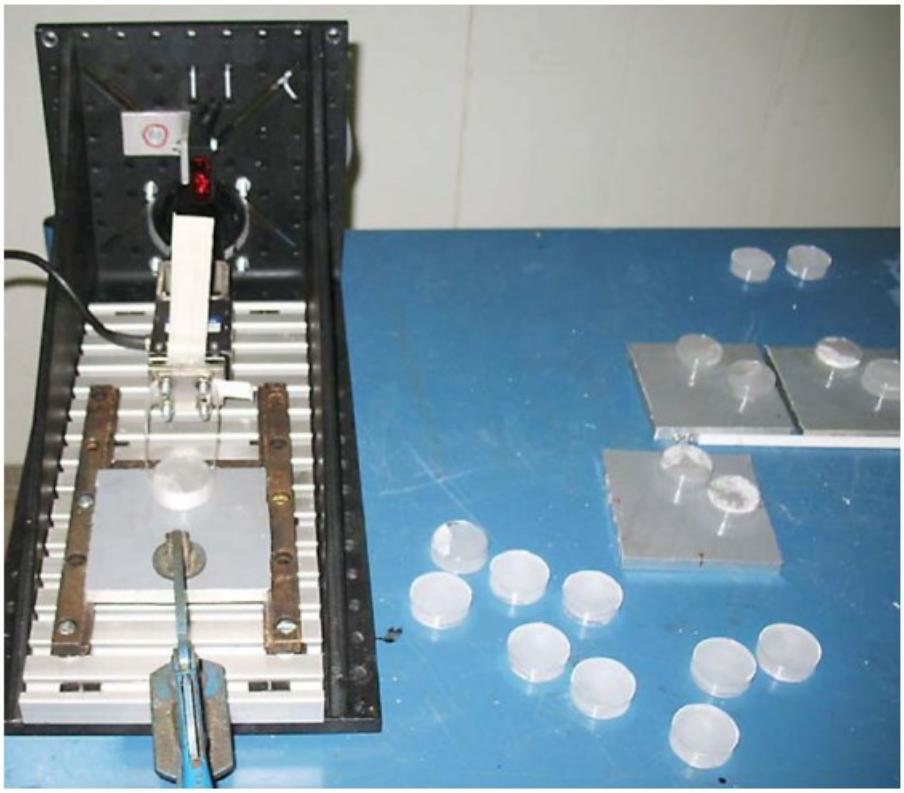

Figure 2.5 The adhesion apparatus used at VTT Finland (Makkonen 2012)

The research by Sobolev et al. on the adherence of rather thick samples of ice to concrete is the next testing setup. Through the improvement of aggregate size, the inclusion of fibers, and the use of super-hydrophobic siloxane admixtures (the latter of which was "a combination of siloxane-based hydrophobic liquid and tiny quantities of super-fine components such as silica fume"), icephobic concrete was created. Two of the methods used by the authors to determine adhesion

strength were splitting and shear testing. The shear test can be seen in Figure 2.6. The authors discovered that a typical shear test was the most accurate for their requirements (Sobolev et al. 2013).

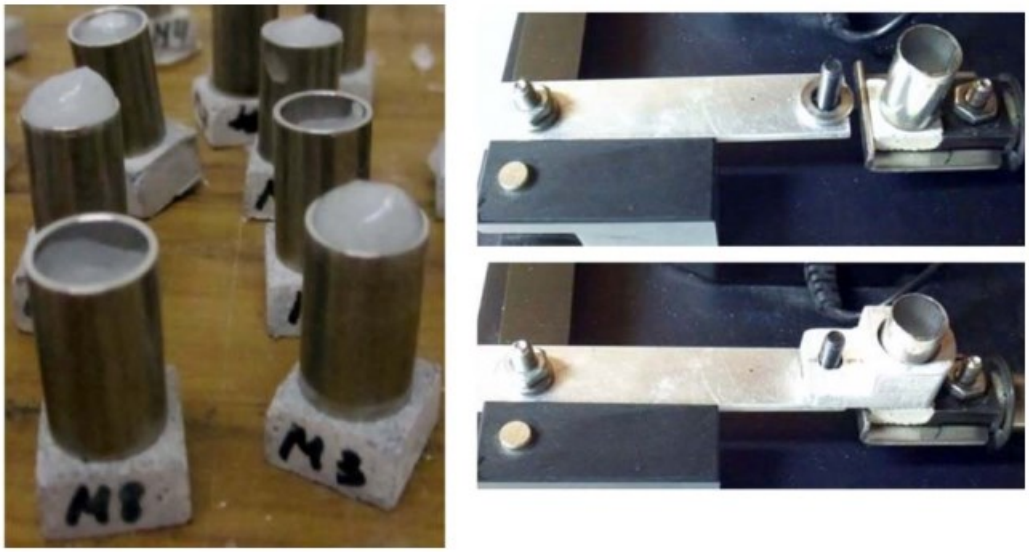

Figure 2.6 Shear test setup on ice and concrete (Sobolev et al. 2013)

In the shear experiments conducted by the authors, the applied force and displacement were measured in order to determine the shear strength. In order to determine the sample area, the inner diameter of the cylinder was used to affix cylindrical ice samples to 15 mm square concrete specimen tiles. Tests were performed at a temperature of −10°C, using prechilled, 0.4°C tap water for the creation of the ice. The researchers discovered that the treated specimens exhibited 10% of the level of ice adhesion as the untreated specimens, especially those with lower cementitious material contents. In the splitting tests, treated samples often failed at the ice-concrete interface while untreated specimens typically failed through the ice sample. Additionally, samples with less cementitious content showed lower adhesive strengths. In general, their final conclusions were that shear strengths with ice ranged from 0.03 to 0.12 MPa for coated concrete samples and from 0.18

to 0.33 MPa for uncoated samples, giving coated concrete samples an overall shear strength with ice of about 1/6 that of uncoated samples.

Greaker's (2014) designed a sliding experiment of five distinct ice samples and concrete. The experimental setup can be seen in Figure 2.7 which the concrete samples were cast five years before to the experiment, kept moist for the first two years, and then exposed to the air.

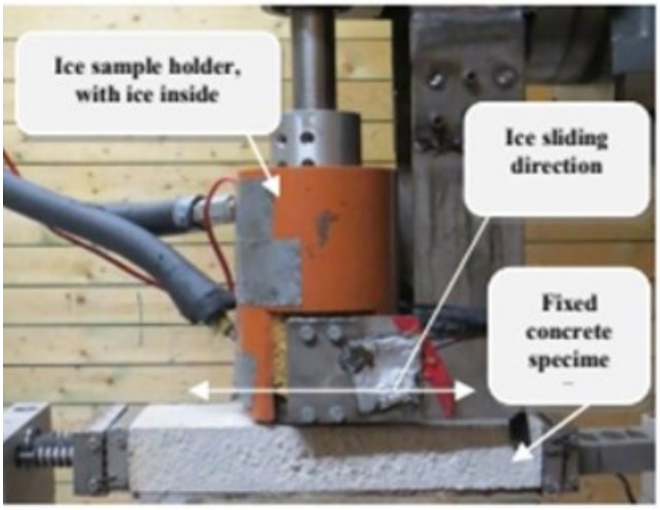

Figure 2.7 Sliding apparatus setup by Greaker (Greaker 2014)

51 MPa was determined to be the average compressive strength. Before and after each test, the surface roughness of 12 concrete sample surfaces—of which 3 had cast surfaces—was quantified using a digital indicator. Ice samples were prepared using tap water, slush and tap water, carbonated water, or drilling from a block of unidirectional ice. They were frozen at various temperatures. The mean abrasion was calculated as the ratio of the mean abrasion depth to the effective sliding distance (Greaker 2014).

Tijsen et al. (2015) tested the effects of normal and sliding movement on ice and concrete where it happened simultaneously. A 30-degree conical ice sample was used for the test, along with two distinct concrete mixtures (high and low performance). These two concrete mixtures' compressive

strengths were calculated to be 70 MPa and 40 MPa, respectively. 180 mm/s24 of sliding velocity and 10 kN of normal force were the respective values. Surface roughness up to 160 micrometers was assessed using a thermal camera (Tijsen et al. 2015).

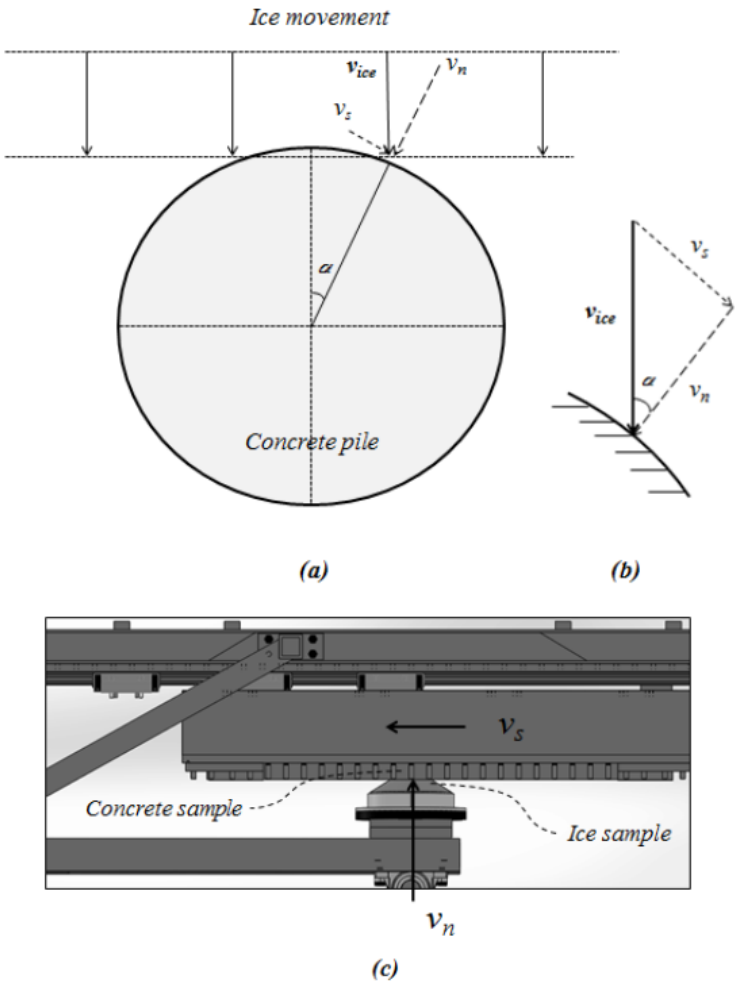

Figure 2.8 "(a) shows an incoming sheet of level ice with ice velocity (v_{ice}) into a circular concrete pile at a point of contact. (b) shows a schematization on local level. The system has two degrees of freedom: ice velocity (v_{ice}) and angle of contact (a), together define the normal velocity (v_n) and sliding velocity (v_s). Figure (c) shows the impingement of the conical ice sample (v_n) and simultaneous sliding of the concrete sample (v_s)" (Tijsen et al. 2015)

Ice buildup on a concrete reservoir embankment and the damage it caused was an incentive for the examination of adhesion strength of ice on concrete by Jia et al. and later Huang et al. (Huang et al. 2017; Jia et al. 2011). Ice samples from the reservoir were tested for shear adhesion on concrete with two roughness values, various displacement rates and five test temperatures. Their test setup can be seen in Figure 2.9.

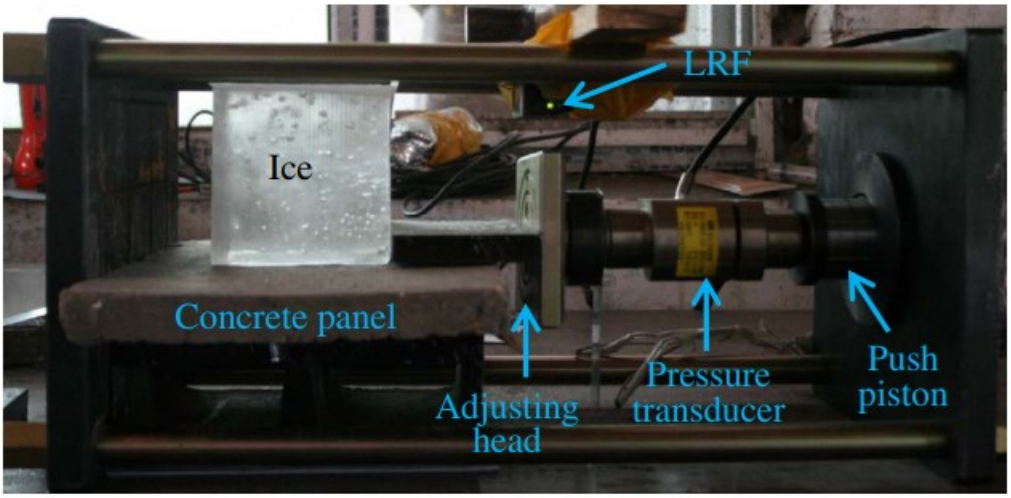

Figure 2.9 Direct shear experiment setup (Huang et al. 2017)

Panel-shaped samples with a surface roughness of 0.3 or 4.2 mm were tested. Testing was subject to a 24-hour bond period. 120 samples were tested in total, each under a basic shear test without the application of an external normal force. The authors identified three distinct types of failure interfaces, including one with little debris associated with high displacement rate failures, one with ice still present on the concrete surface associated with low displacement rates, and one with some concrete damage and debris stuck to the ice, which the authors attributed to both the adfreeze bond strength and the cohesion of the concrete. The adhesion strength increased with lowering specimen temperature during tests with test temperatures ranging from 2°C to 10°C. Concrete that was coarser had adhesion strengths that were around 30–40% greater than concrete that was smooth.

Although there have been many different kinds of adhesion tests, the authors pointed out that there are presently no standardized testing methods. Although the values of their study were usually in accord with others, the comparison the authors made with earlier test programs revealed that there was a broad range of outcomes. Their results were inconclusive and scattered in most parts and some general conclusion could be made. Direct comparisons were challenging due to varying testing conditions, such as the application of a typical, confining force for straightforward shear tests or lateral confinement in other experiments. Finally, They also concluded that when the weak peaks, where the displacement rates were around 10^{-2} mm/s and the loading rates were 1–10 kPa/s, were disregarded, the adfreezing strengths were independent of the displacement rates and loading rates.

Experimental research was created by Pramanik (2021) to determine the strength of the adhesion connection between mid-strength concrete and freshwater ice under varied contact pressure and duration conditions at a constant temperature of -1°C. Both dry and (one) submerged tests were performed as part of the research. A nonlinear relationship was found for adhesion strength with various contact pressure and duration. Adhesion was observed to be higher in the submerged test than the corresponding dry test. Finally, For each test, a low average rate of concrete abrasion was discovered (Pramanik 2021).

2.3 Relation between Water Contact Angle and Ice Adhesion

There can be various ways to explain the theory of ice adhesion. Makkonen has explored the basic theory behind contact angle and ice adhesion (Makkonen 2012). Think of a water droplet (w) on a solid (s) with an interface (w, s), surface energy (γ), and a droplet contact angle (θ). The scenario is schematically represented in Figure 2.10.

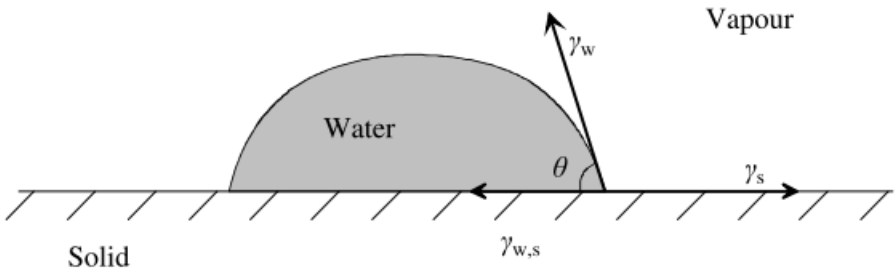

Figure 2.10 The definition of the contact angle θ (Makkonen 2012)

The equilibrium of this condition is described by the Young equation:

$$\gamma_{w,s} + \gamma_w \cos\theta = \gamma_s \qquad \textbf{2-1}$$

Think about the ice (i) that is frozen on the solid (s). This would imply that the drop in Figure 2.10 had turned into ice. We are now interested in the work that must be done to break the bond (i,s) and create two new surfaces (i and s) without considering deformations in order to remove the ice. we refer to it as the thermodynamic work of adhesion, or W_a:

$$W_a = \gamma_s + \gamma_i - \gamma_{i,s} \qquad \textbf{2-2}$$

Inserting γ_s from Eq. **2-1** to Eq.**2-2** shows that:

$$W_a = \gamma_i + \gamma_w \cos\theta + (\gamma_{w,s} - \gamma_{i,s}) = \gamma_s \qquad \textbf{2-3}$$

Assuming that the surface energies of water and ice are roughly equivalent and assuming that their interfacial energies at the solid interface are also approximately the same, we may calculate:

$$W_a \approx \gamma_w (1 + \cos\theta) \qquad \textbf{2-4}$$

Eq. **2-4** states that the surface tension of water and the angle at which it contacts the medium can approximately reflect the thermodynamic work of ice adhesion. Figure 2.11 provides a visual representation of this. Equation **2-4** and Figure 2.11 demonstrate that, in theory, we should

anticipate a deterministic dependency between the work of adhesion and the water contact angle in the process of removing ice. Finding a divergence from the Figure 2.11 curve in macro-scale studies would possibly suggest that materials are deformed, or that the ice-solid contact is complicated or imperfect in some way.

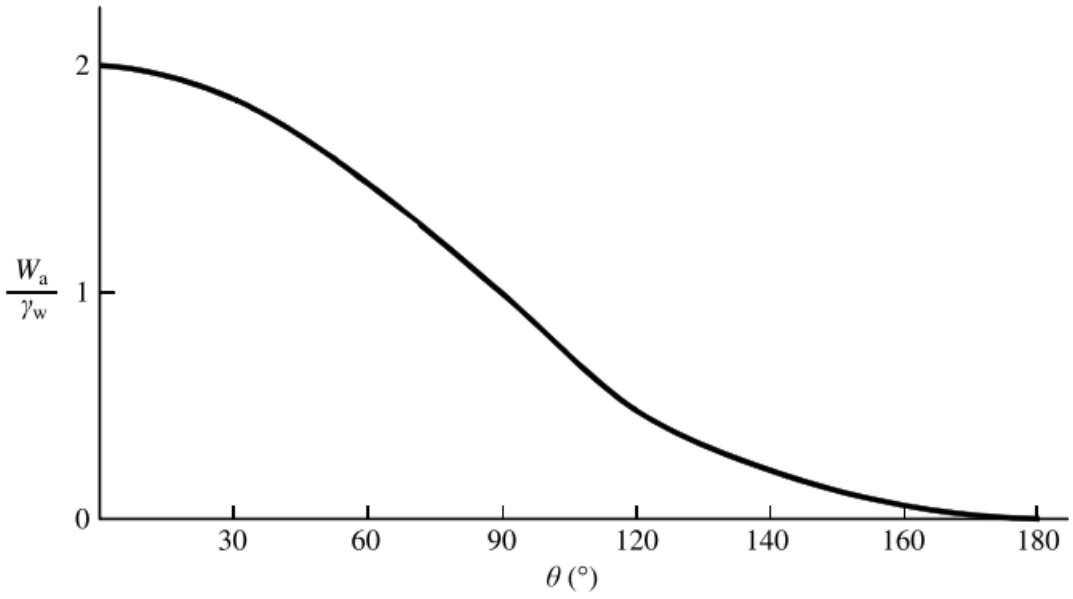

Figure 2.11 "Thermodynamic work of ice adhesion scaled by the surface tension of water as a function of water contact angle θ" (Makkonen 2012)

2.4 Dual-crystallization Waterproofing Technology for Topical Treatment

The material investigated in this study is Chem-Crete PAVIX CCC100, (referred to PAVIX throughout the thesis) a patented Dual-Crystalline. Here is a brief description of the material. A patented mixture of many reactive ingredients in an aqueous solution makes up the dual crystallization waterproofing engineered (DCE) substance, which is sprayed over freshly poured concrete , as well as completely cured or older concrete (Al-Jabari 2022). The solution is water-based with low viscosity that allows its penetration into the concrete structure. Depending on the

variation of the coarse particles positioned close to the surface of the specimen, measurements of penetration depths for concrete specimens revealed that the product reaches between 0.13-0.254 inches. The rise in chemical concentration brought on by water-carrier evaporation triggers and/or speeds up the many, simultaneous chemical reactions that occur within the concrete capillaries at such a depth. The formation and performance mechanism are depicted schematically in Figure 2.12.

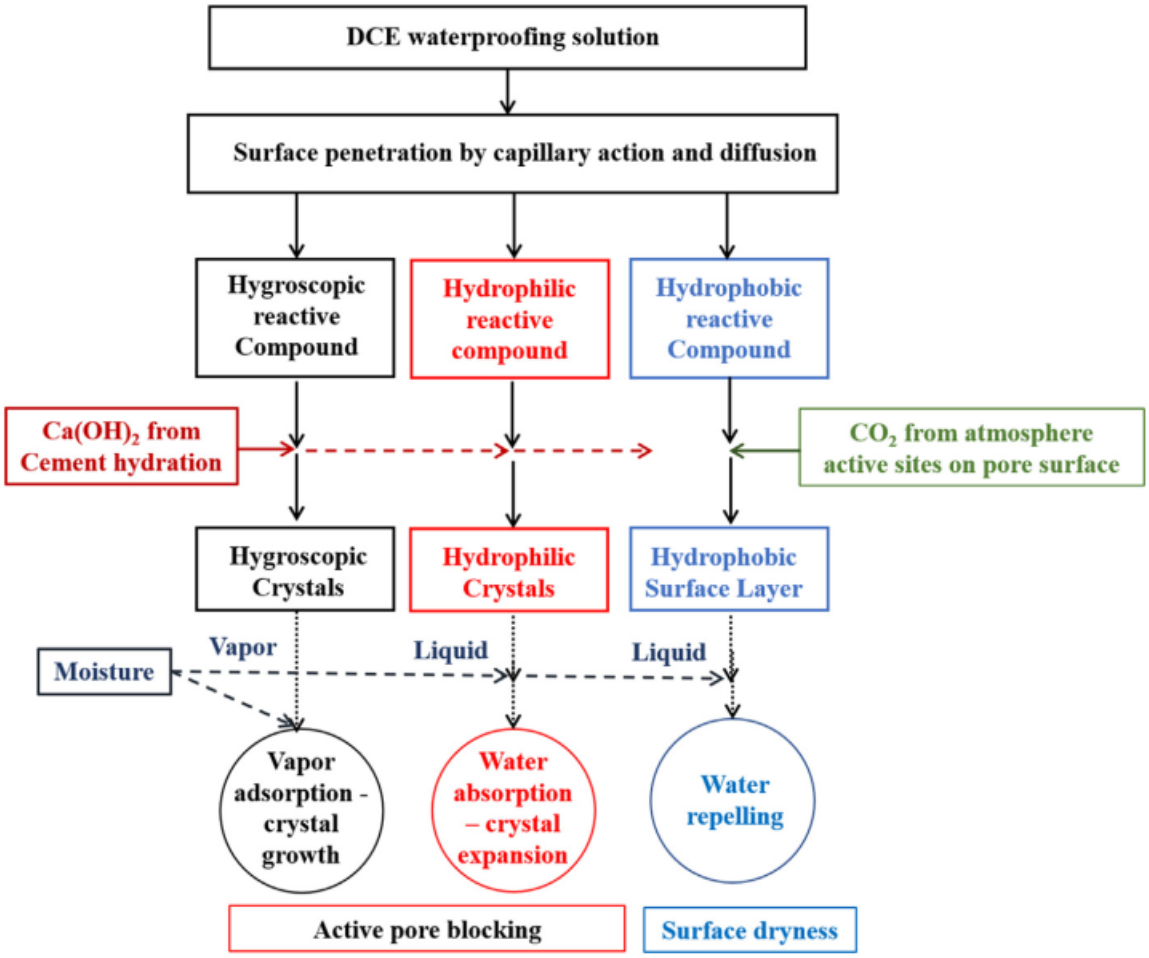

Figure 2.12 A schematic representation of the formation of the DCE system and its performance mechanism (Al-Jabari 2022; Al-Rashed and Jabari 2020)

By creating a crystallization system that fills and blocks the gaps and capillary network and has hygroscopic, hydrophilic, and water repellent properties, the resultant crystals reduce water transport through the concrete matrix. Concrete surfaces are treated with the DCE solution using a brush or a sprayer. Two different kinds of spraying equipment utilized in industry are seen in Figure 2.13.

Figure 2.13 Application of the DCE solution by spraying onto cured concrete for an airport runway (A) and a pavement (B) (Al-Jabari 2022)

Further information can be access by referring to the recently published book “Integral Waterproofing of Concrete Structures” by Dr. Maher Al-Jabari in 2022.

2.5 Summary of the State of the Art

Ice contact is one of the main causes of the surface abrasion of marine structural concrete in colder climates. For concrete buildings such as lighthouses, docks, bridge piers, or guide walls, abrasions are discovered close to or at the waterline. The strain rate, salinity, crystal orientation, and temperature are the main determinants of the actual strength of the local ice force. Moving ice may occasionally cause marine constructions to sustain catastrophic damage, eliminating all of the concrete covering at the waterline (B. C. Gerwick and Jr. And D. Berner 1988). The ice load and concrete resistance need to be monitored in order to precisely detect the concrete abrasion mechanism and the wear rate. It is necessary to measure the physical and mechanical characteristics of both ice and concrete as part of both field and laboratory research. Additionally, before a test plan is created and data is gathered during experimentation, the physical characteristics of the interaction need to be carefully considered (Barker et al. 2021; Jacobsen et al. 2015).

Ice adhesion, ice friction, and concrete wear caused by dynamic interactions with ice have all been widely studied in general. However, the research conducted is not focused on specific problems like pavement ice removal, there is a lack of coherency in the testing methodologies, goals, and solution for further alleviation of the various problem.

Chapter 3 Laboratory Investigations

3.1 Materials and Test Specimens

A standard TxDOT concrete, commonly used for bridge slabs, top slabs of direct traffic culverts, and approach slabs in Texas, is selected as the concrete mix to make the concrete specimens needed for this study. This type of concrete has a minimum compressive strength, f'_c= 4000 psi. A local concrete supplier delivered the concrete mix on-site, where all the test samples were prepared. Water-cement (w/c) ratio of 0.45 is the maximum ratio specified in the TxDOT specifications. In addition, a lower w/c ratio of 0.43 was applied to the concrete mix to study the effect of w/c on the concrete properties.

Four-inch concrete cylinder samples were cast on the 17th of May 2021 following ASTM C31/C31M-21a as shown in Figure 3.1. Some samples which were to be tested for specific heat capacity had embedded type T thermocouples during casting. After the casting, all the concrete cylinders were kept in a standard moisture curing room before further testing and treatment. Some of the concrete cylinders were selected for PAVIX treatment, which was performed in a room outside of the moisture room on the 26th of July 2021. The PAVIX treatment was performed by spraying PAVIX CCC100 on the concrete cylinder top surface following the manufacturer's recommendation with a surface coverage of 150 ft^2/gal, which roughly equals 3.7 m^2/l. The treated cylinders were allowed to cure for 24 hours before being transferred to the moisture room. The untreated cylinders and PAVIX-treated cylinders were stored in the moisture room with molds before they were de-molded and processed for making ice-adhesion specimens, which were performed within a period from January to March of 2022.

Figure 3.1 Concrete cylinders with and without Type-T thermocouple

Three-gang plastic mold forms 2x2in (51x51mm) were used to cast cubic samples, as shown in Figure 3.2. Similar to the concrete cylinder samples, PAVIX-treatment was performed on the same following the same procedure. All the cubic samples, including control and PAVIX-treated, were used in contact angle measurements.

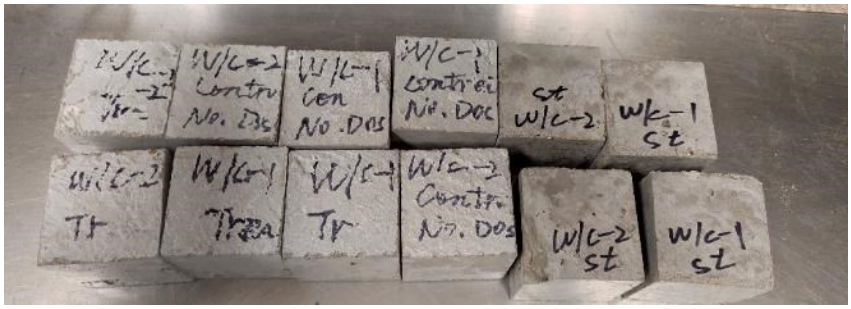

Figure 3.2 Cubic concrete samples for contact angle test

All the concrete cylinder samples have two different water-to-cement ratios: 0.45 and 0.43. The identification (I.D.) is assigned to each tested cylinder as follows. A specimen I.D. is explained in Figure 3.3. The ID is followed throughout the study for clear identification of each test specimen. In this manner, the water-to-cement ratio, the sample type, cylinder number and whether the specimen is cut from previously used cylinders can be discerned.

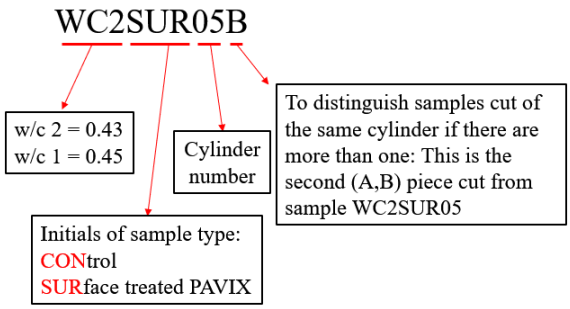

Figure 3.3 Specimen ID explanation

The entire test specimens used for this study for each w/c ratio can be seen in Table 1.

Table 1 All test specimens used in the project for each w/c ratio

For Each w/c Ratio		Number of Specimen*	Test Condition
Type of Test	**Test Sample**		
Shear Test for Ice-Adhesion	Control Concrete Cylinder	3	30 °F
		3	13 °F
	Concrete Cylinder with Surface Treated by PAVIX	3	30 °F
		3	13 °F
Contact Angle	Control Concrete Cube	1	Room temperature
	Concrete Cube with Surface Treated by PAVIX	2	
Thermal Conductivity	Control Concrete Cylinder	2 (6 Tests)	
Specific Heat Capacity	Control Concrete Cylinder	2 (4 Tests)	

* Each specimen was tested once for ice-concrete adhesion or contact angle

3.2 Ice Adhesion Test

3.2.1 Test Program

The removal of ice from the road surface by a snowplow is achieved by shearing. Therefore, a customized direct shear box from Geocomp, is adopted to measure ice-concrete adhesion. A hollow aluminum block is designed for making an ice disc on top of a concrete disk. This ice-concrete disc is sheared laterally at the ice-concrete interface with the lateral force provided by a step motor. During shearing, the resistance load and displacement of the ice block are recorded to determine the maximum ice-concrete adhesion.

Ice adhesion tests were performed by shearing ice-concrete specimens using a modified direct shear box inside a temperature-controlled freezer box at freezing. This includes concrete disk specimen of control type of the both water-to-cement ratios, and PAVIX-treated disks of the same concrete as well. Ice-concrete test specimens were prepared inside a freezer at controlled temperature for 24 hours before shearing. This would allow the ice formation on top of the concrete disk. Then the direct shear apparatus was moved inside the freezer to run the shear tests on the prepared ice-concrete specimens. The test program of ice adhesion shear tests can be seen in Table 2 and

Table 3. The treated concrete specimens are referred as PAVIX-treated in the rest of this study. As there can be inherent variance regarding the properties of samples with similar water-to-cement ratios, some control specimens were cut from the same cylinder with surface treatment of PAVIX on a lower untreated section if possible. This would allow the comparison of treatment of specimen cut from the same cylinder with the same properties, taking into consideration that the control

surface is smooth after cutting while the treated surface is rough as obtained from the top surface of the casted specimen, as detailed below in the test procedure section.

Table 2 Ice adhesion test program for water-to-cement ratio 0.45

For w/c= 0.45		Specimen ID	Test Condition	Number of Tests (One test for each specimen)
Type of Test	**Test Sample**			
Shear Test for Ice-Adhesion	Control Concrete Cylinder	WC1SUR04B	30 °F	3
		WC1SUR05B		
		WC1SUR06B		
		WC1CON02B	13 °F	3
		WC1SUR01B		
		WC1SUR03B		
	Concrete cylinder with Surface Treated by PAVIX	WC1SUR04A	30 °F	3
		WC1SUR05A		
		WC1SUR06A		
		WC1SUR01A	13 °F	3
		WC1SUR03A		
		WC1SUR02A		

Table 3 Ice adhesion test program for water-to-cement ratio 0.43

For w/c= 0.43		Specimen ID	Test Condition	Number of Tests (One test for each specimen)
Type of Test	**Test Sample**			
Shear Test for Ice-Adhesion	Control Concrete Cylinder	WC2SUR04B	30 °F	3
		WC2SUR06B		
		WC2SUR05B		
		WC2SUR02B	13 °F	3
		WC2CON07A		
		WC2CON06A		
	Concrete cylinder with Surface Treated by PAVIX	WC2SUR05A	30 °F	3
		WC2SUR04A		
		WC2SUR06A		
		WC2SUR01A	13 °F	3
		WC2SUR02A		
		WC2SUR03A		

3.2.2 Test Procedure

Ice-adhesion tests were performed on a Geocomp ShearTrac-II direct shear without the vertical module, i.e. no normal load to the shearing interface. The load cells and LVDTs used in the direct shear apparatus were thoroughly checked for temperature calibration. The sensors are compensated for temperature. Besides, PAVIX-treated specimens were tested with their control specimens in one test set under same temperature to further eliminate any temperature induced bias, if any.

The direct shear apparatus is shown in Figure 3.4. The concrete specimen used for these tests are disks of about one inch height cut from concrete cylinders. To test the effects of PAVIX surface treatment, the top surfaces of the PAVIX-treated concrete cylinders were used to measure their ice-adhesion. The test specimen was obtained by cutting the cylinder at one inch from the top surface. In most cases, the rest of the same cylinder was used for control specimens as the concrete material is almost identical to the PAVIX-treated one for a better and more accurate comparison of the effects of the treatment. Figure 3.5 demonstrates the process of preparing PAVIX-treated concrete discs.

Technical Specifications

LOAD CAPACITY

Up to 11 kN (2.5 klbf) vertical and horizontal

VERTICAL/HORIZONTAL MOTORS

Micro-stepper system with built-in controls

CONTROL

- Stress (load)
- Strain (displacement)

RATE OF DISPLACEMENT

0.000006 to 33 mm/min
(0.0000002 to 1.3 in/min)

Figure 3.4 Geocomp ShearTrac-II direct shear apparatus and its specifications

It shall be noted that the ice formation and shearing tests on the control specimen were done on the cut surface of the concrete disk. In contrast, for PAVIX-treated disks, ice was formed and sheared on the top rough surface of the specimen. It is known that rough surfaces have higher bond strength with ice as compared with cut smooth surface. Figure 3.6 explains the steps of making ice-concrete specimens for direct shear test. Three molds were prepared for making ice-concrete specimens in one test run; the ice-concrete specimens were sheared consecutively. Therefore, the three test specimens in the same set had the same temperature during ice-making and shearing processes. The steps of making and shearing specimens are shown below.

1) Cut three disks from specific cylinders
2) Prepare the concrete disk surface to be bonded with ice; mark the area to be bonded with ice as shown in Figure 6; grind off rough edges to ensure no contact of upper sample holder against the concrete disk; the grinding does not happen on the surface area where ice was to be formed and had no effect on the ice adhesion; for PAVIX-treated discs, the area to be bonded ice remained intact to preserve the original surface texture

3) Apply grease to the concrete surface to allow proper contact between the aluminum mold and concrete surface; it shall be applied with care to ensure it is watertight while no extra grease remained inside the mold; then the mold is filled with water
4) Set the freezer box to the set testing temperature 13 °F or 30 °F
5) Transfer the 3 samples into the freezer when the set temperature is reached
6) Allow 24 hours for ice-formation before shearing the specimens

Figure 3.5 PAVIX-treated specimens, sample disks cutting and preparation

Figure 3.7 and Figure 3.8 show the schematics and pictures of ice-concrete specimens and the test setup in the direct shear apparatus, respectively. The ice-concrete disc is placed inside the direct shear box with concrete disk on the top. The top disc is hold fixed with a custom-made aluminum sample holder. The bottom aluminum used for making ice is set inside the direct shear box which is connected a step motor. During the shearing test, the bottom ice disc is moving while the top concrete disc is fixed. As mentioned previously, the direct shear apparatus and its P.C. was moved inside the freezer box when running shearing test at freezing temperature. The schematics of the ice adhesion test inside the freezer box can be seen in Figure 3.9. As shown, the sample is sheared

with ice on the bottom. The direction of the shearing can also be seen in the schematic. The insulated apparatus with a P.C. inside the cart can be seen in Figure 3.10.

Cut Disks

Samples Ready to Be Filled and Frozen

Control Disk with Cut Surface

PAVIX-Treated Disk with Rough Surface

Figure 3.6 Some steps of specimen preparation

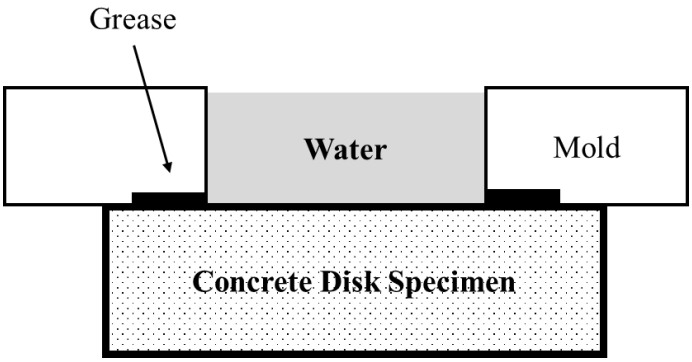

Figure 3.7 Schematic of the ice-concrete specimen preparation

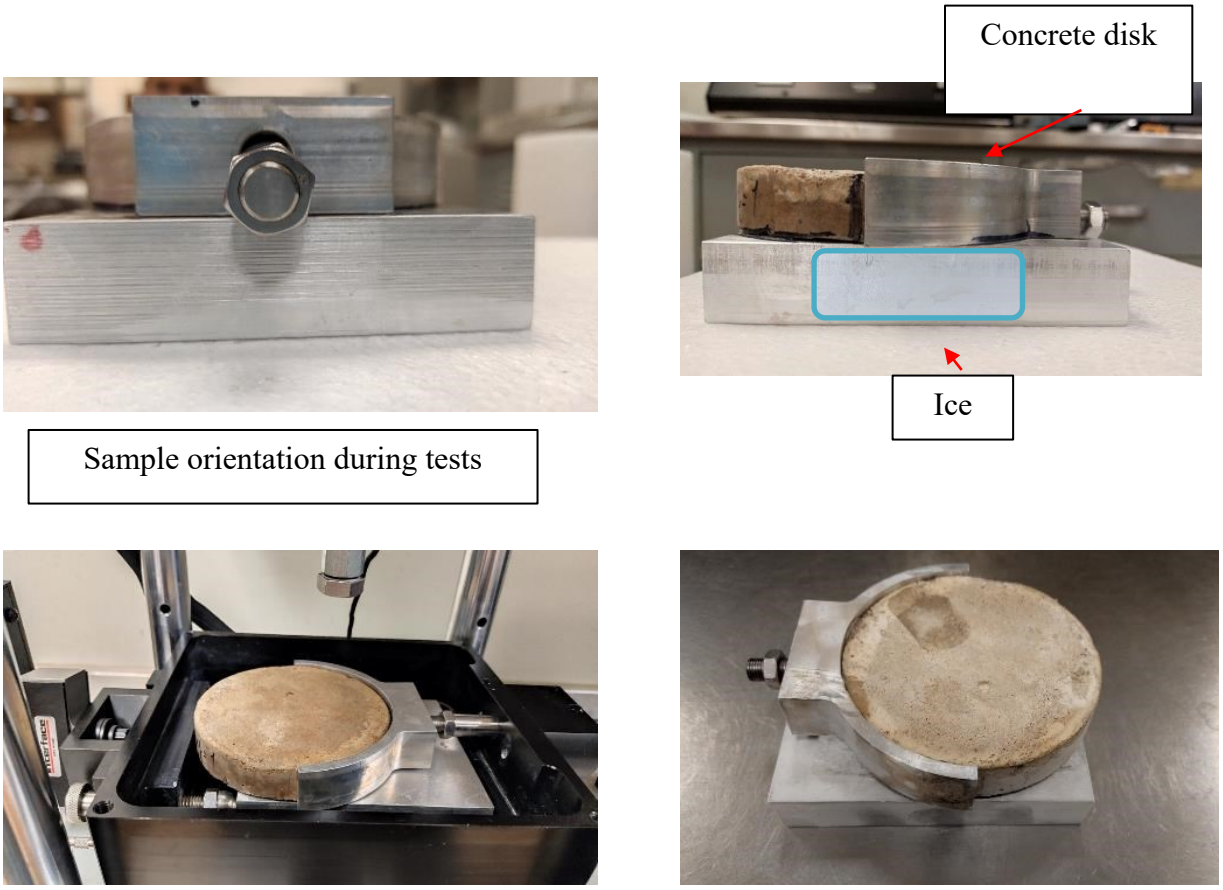

Figure 3.8 Final specimen; its mold, orientation, and test location

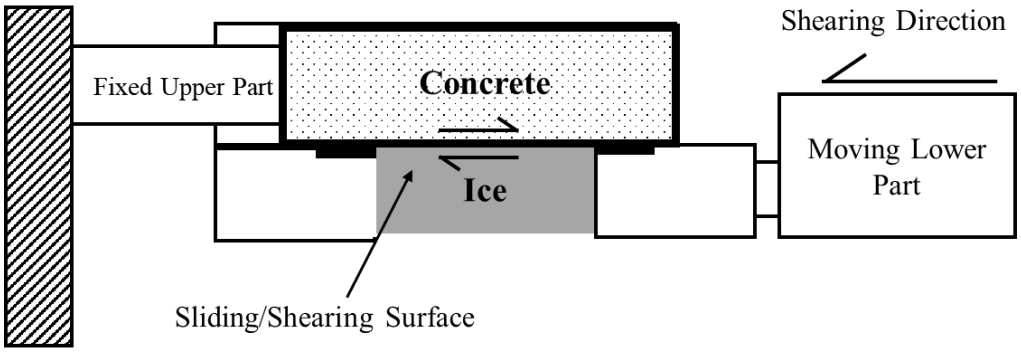

Figure 3.9 Schematics of the ice adhesion shear test inside the freezer box

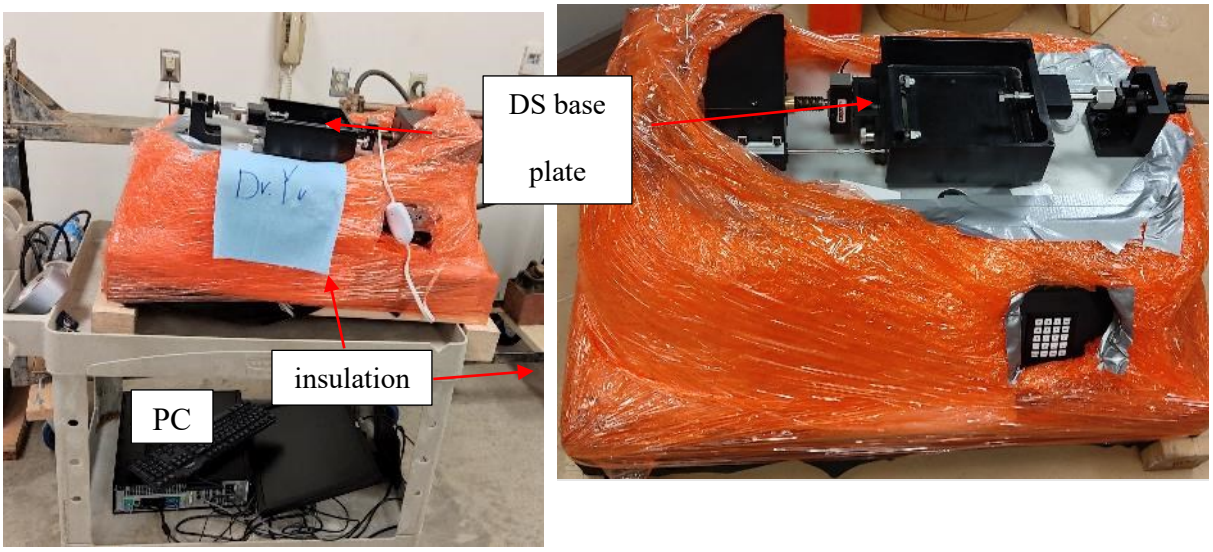

Figure 3.10 Portable direct shear apparatus insulation and its preparation

The final testing site with the direct shear apparatus inside the freezer and its P.C. set up can be seen in Figure 3.11.

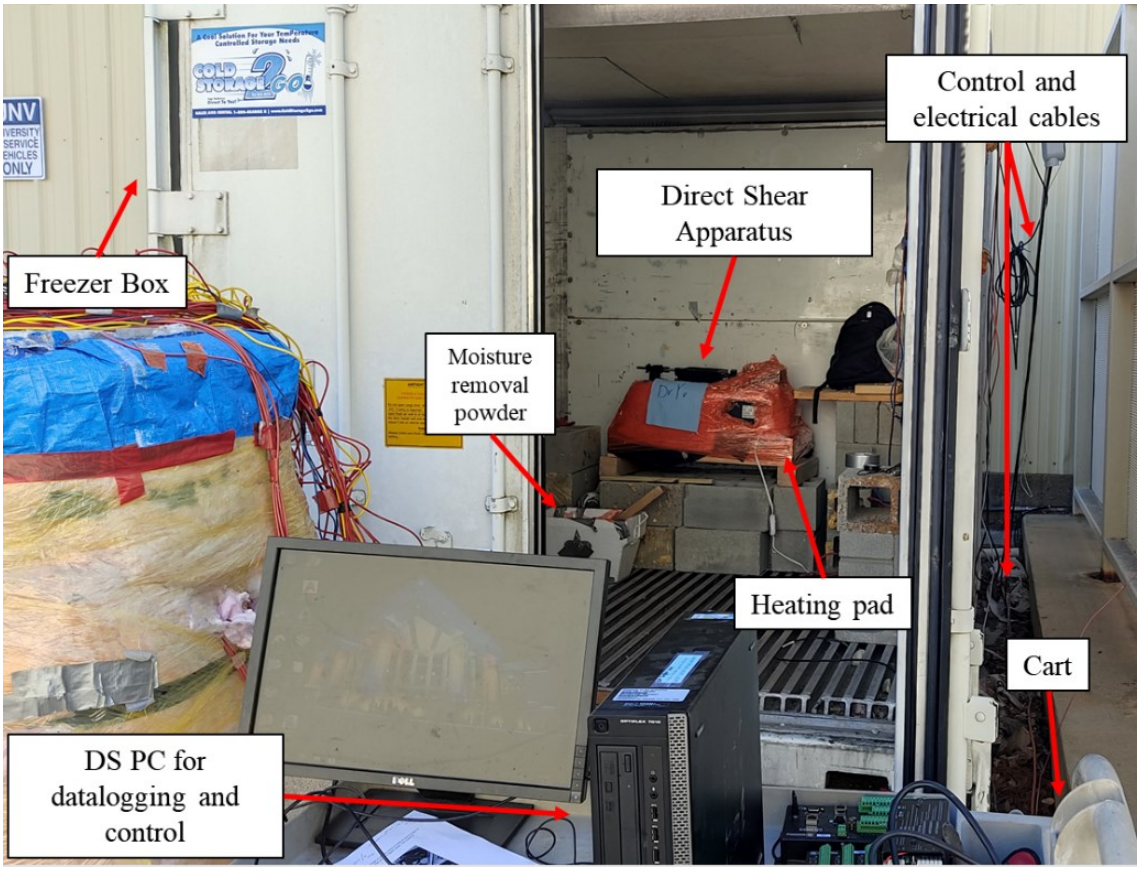

Figure 3.11 Ice adhesion test setup inside the freezer box

In Figure 3.12, the direct shear apparatus ready to be tested can be seen inside the freezer box. One thermocouple records the temperature of the direct shear box where specimen is put for testing on the apparatus and the other records the ambient temperature. This allows for verification of the temperature during ice sample preparation and shearing. It is noted that the tests were all run in a strain control mode. The strain speed is constant during all the tests and is 33 mm/min which is the maximum strain speed of the apparatus. The strain rate can directly affect the ice adhesion value and the reason the maximum speed is chosen is because the ice removal process on roads with a snowplow is a very fast process. To avoid any strain rate effects, this rate is kept constant throughout all tests.

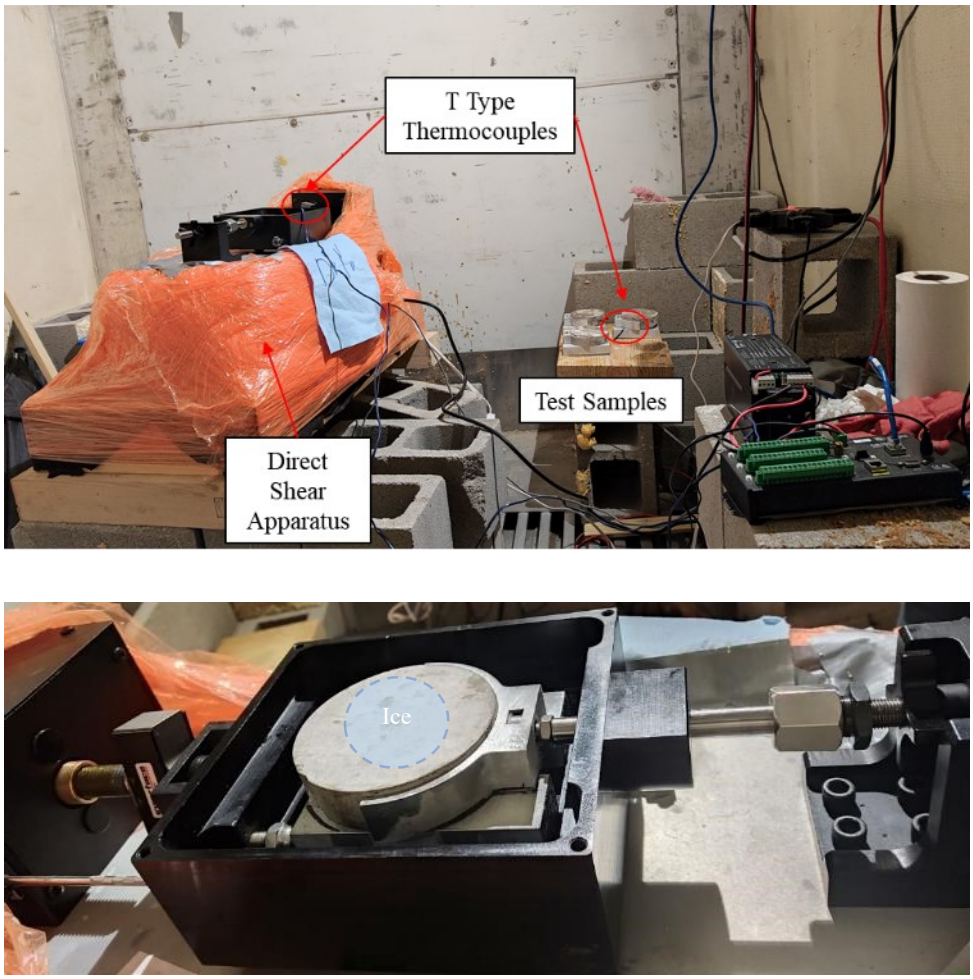

Figure 3.12 Setup inside freezer box during the test

3.2.3 Sample Test Results

The shearing result of the test performed on disks IDed WC2SUR01A and WC2SUR01B which is tested at 13 °F can be seen in Figure 3.13. There are various criteria for failure regarding shearing and what displacement would be considered failure. Throughout all the tests a displacement limit of 0.4 inch which roughly corresponds to 16% of ice diameter is chosen as an excessive displacement after which it can be assured failure has happened already. This number for conventional direct shear tests is 10% corresponding to 0.25 inch. The direct shear result with a

steep curve correctly conveys the very stiff nature of the sheared material as ice is brittle and upon shearing would break off from the concrete.

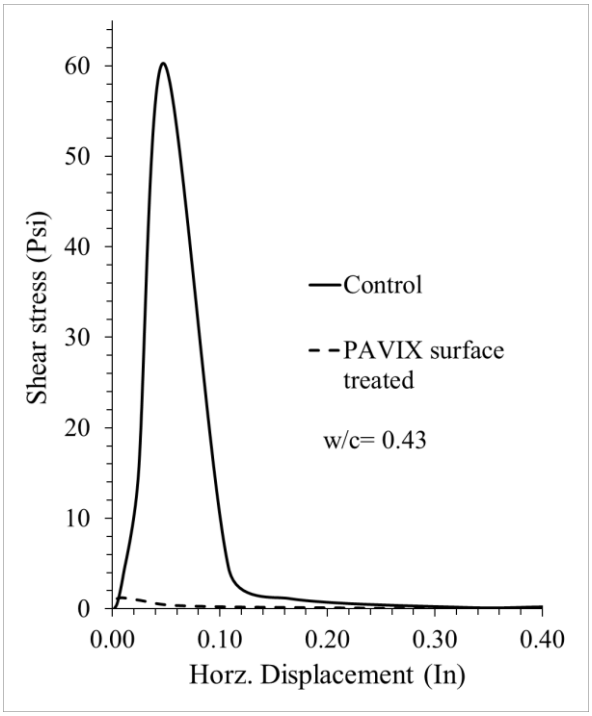

Figure 3.13 Ice adhesion test result on two specimens cut from WC2SUR01 in 13 °F

The cylinder WC2SUR01 was surface treated with PAVIX material. Specimen WC2SUR01A is the top one-inch part cut from the cylinder and specimen WC2SUR01B is a disk cut below that from the same cylinder. The second disk would be the control specimen with identical concrete specifications but without any top treatment. The peak value of the shear stress is used as the ice adhesion value, indicating when the ice would break off from the concrete surface. In this case this value is 60.2 psi. This sample value which roughly corresponds to 415 kPa is well within range of the reported values of ice adhesion to typical concrete surfaces (Jia et al. 2011). Of course, the shearing rate, the ice formation and testing temperature all affect the ice adhesion value. Furthermore, a data logger with type T thermocouples was used to monitor the temperature of the

freezer box to ensure uniform temperature was maintained. A whole span of more than 24 hours, from samples being put inside the freezer until the testing period for set 4 tests is shown in Figure 3.14. A more detailed temperature curve from the moment the freezer box was opened to be checked and to perform the test until the freezer box was turned off can be seen in Figure 3.15. The average freezer temperature (ambient) during ice-making process and shearing, and average direct shear plate temperature during shearing are reported in the Appendix.

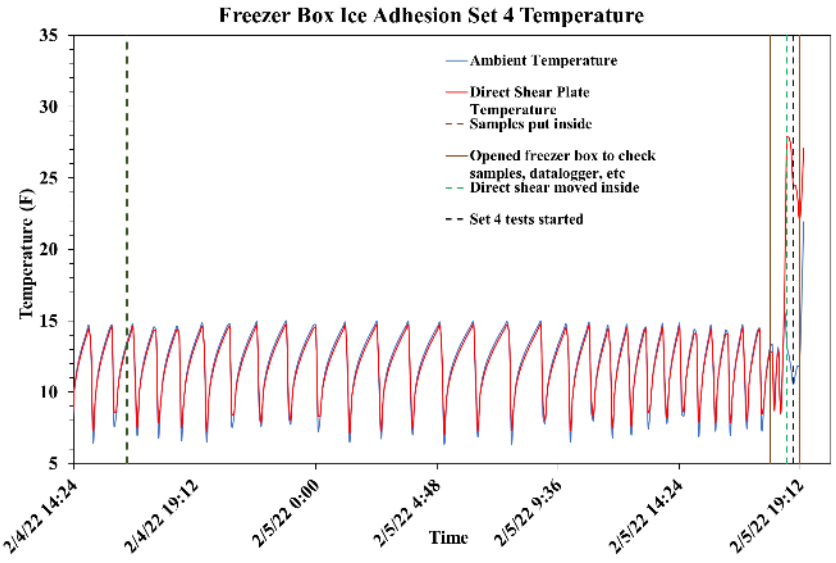

Figure 3.14 Sample monitored temperature curve from ice formation to test performance

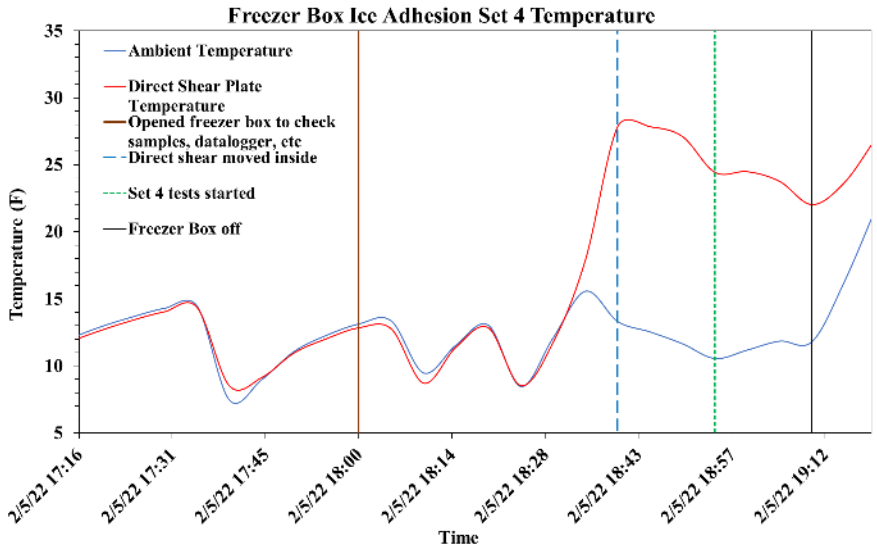

Figure 3.15 Sample monitored temperature curve during a test

3.3 Contact Angle

Contact angle as the angle a drop of water forms on the surface of the concrete can be used as a property to measure hydrophobicity of a surface. To better understand this idea, please refer to the 2.2 section of this study. Samples of treated and untreated concrete were tested for this.

3.3.1 Test Program

The objective of this test is to quantify the effect of PAVIX CCC100 on concrete surface wettability using contact angle (static and dynamic) as an indicator. The test program for contact angle measurements is summarized in Table 4. A total of 6 measurements were conducted for all four specimens. Static contact angles were measured on August 8, 2021, and all dynamic contact angles were measured on October 7, 2021. The contact angle was measured approximately 1-2 seconds from the time of placing the drop on the concrete surface. This measurement time was used to mitigate the influence of evaporation and droplet movement on contact angle measurement. It is reported from literature that contact angle decreases as time elapses between placing the drop

and reading of the contact angle. For control samples, only static contact angle was measured since the surface of the control sample is hydrophilic; it was difficult to photo water droplets on a tilted sample surface.

Table 4 Summary of contact angle measurement test program (Hashemi Senejani, Lei, Yu 2022)

Test ID	Specimen	Water cement ratio (w/c)	Contact angle	Number of measurements
1	Control	0.45	Static	1
2	Surface Treated by PAVIX		Static & dynamic	2
3	Control	0.43	Static	1
4	Surface Treated by PAVIX		Static & dynamic	2

3.3.2 Test Procedure

Measuring the contact angle of treated and the non-treated concrete specimen is essential since it is related to the performance of hydrophobicity and icephobicity, as water drops may bounce back when they impact a hydrophobic surface (Di Mundo et al. 2020). Surface treatment was performed around 60 days after the casting of the specimens meaning on fully cured concrete cylinders. PAVIX CCC100 was sprayed over the top surface of the cube specimens with them inside the mold. The treatment was performed with a ratio equivalent to 0.2 mm liquid film thickness on top of the treated areas (equivalent to a coverage rate of 150 sq. ft per gallon). The cube samples were removed from the molds and cut for thin sections, as shown in Figure 3.16. The thin sections were

prepared using a stone cutting machine and at 5 mm thick and 5 cm square. Some sections were partly broken during the cutting process. Contact angle measurements of the thin sections were performed using a Goniometer/Tensiometer (Ramé-hart Model 250), as presented in Figure 3.17. It is worth to mention that for the PAVIX treated concrete, the contact angle may decrease with depth (for lower cut sections) and with the mechanical action of the cutting.

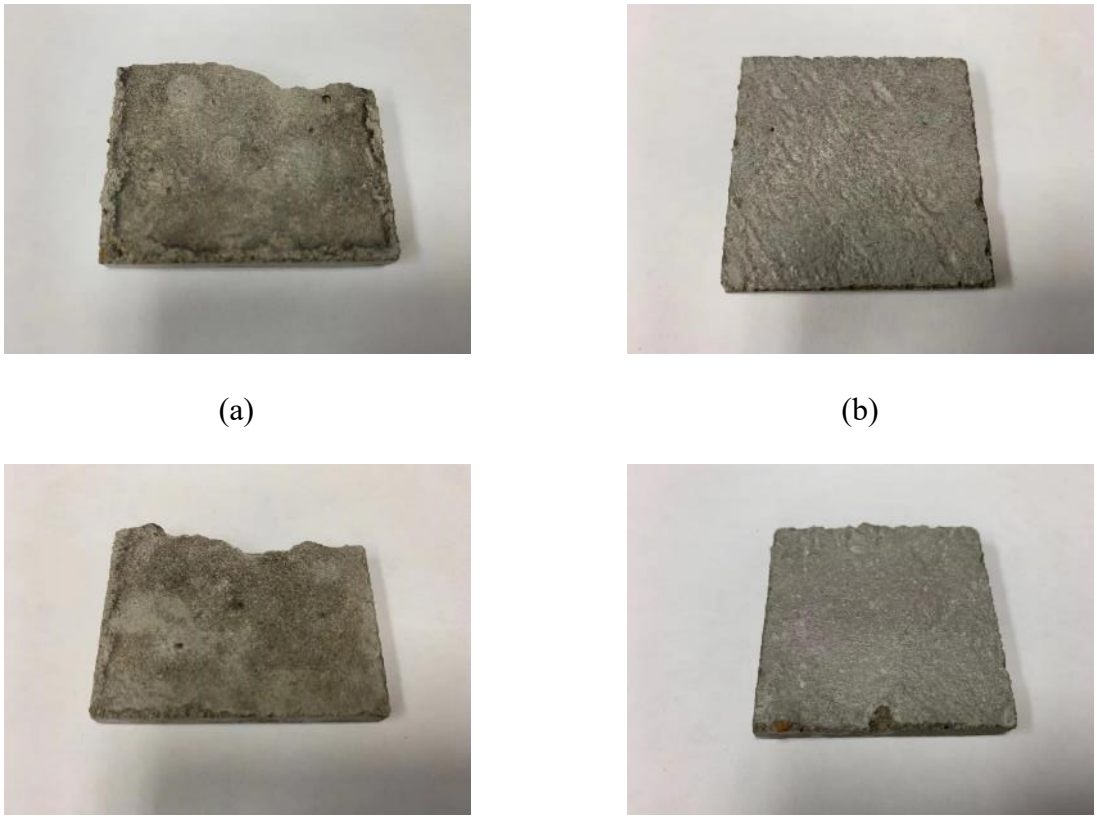

(a) (b)

(c) (d)

Figure 3.16 Thin sections stemming from different concrete cubic blocks: (a) control sample with w/c= 0.45, (b) top treated sample with w/c= 0.45, (c) control sample with w/c= 0.43, and (d) top treated sample with w/c= 0.43.

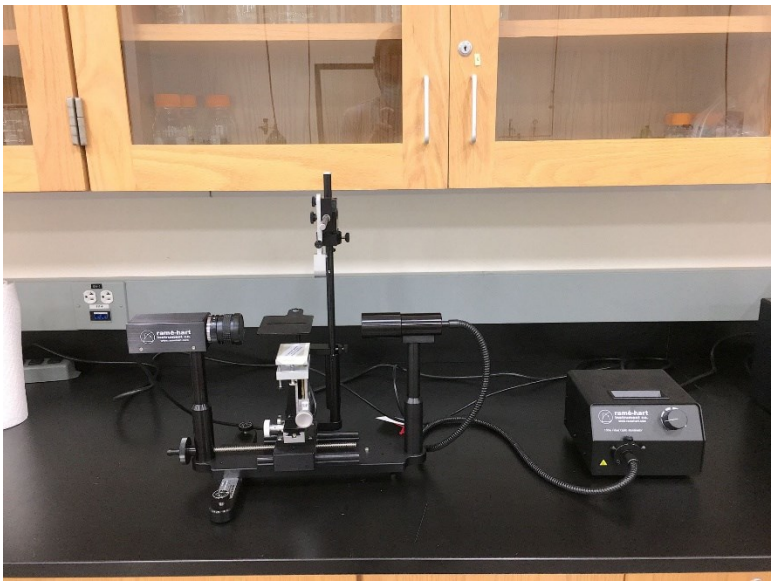

Figure 3.17 Goniometer/Tensiometer (Ramé-hart Model 250)

The sessile drop method (S.D.M.) was adopted to measure the contact angle of a water droplet on a concrete surface. The assumptions of this method for concrete contact angle measurements are that gravitational effects on the drops are negligible, the concrete surface is relatively smooth, and the heterogeneity of the concrete surface is limited. The procedures of S.D.M. for measuring static contact angle are as follows: (1) placing the target concrete thin section with a relatively smooth surface on a goniometer's stage and dispensing a pre-determined volume of deionized water droplet on the sample. The volume of drop usually ranges from 1 to 2 µl (Lourenço et al., 2018) but drop volumes up to 20 µl can also be adopted (Buczko and Bens, 2006). (2) Recording the water droplet on the specimen surface at approximately 1-2 seconds after the droplet is released. (3) Measuring contact angle by a fitting outline of droplet and baseline by using ImageJ software. The improvements of the contact angle determination were also performed by applying the Low-Bond Axisymmetric Drop Shape Analysis (LBADSA) method (Stalder et al. 2010), which was integrated into a plugin of ImageJ. The difference between the static and dynamic contact angle measurements is that the specimen will be tilted to a critical angle that the water droplet is nearly

to fall from the on the specimen surface, as shown in Figure 3.18. Both static and dynamic contact angles were measured for the specimens in this study.

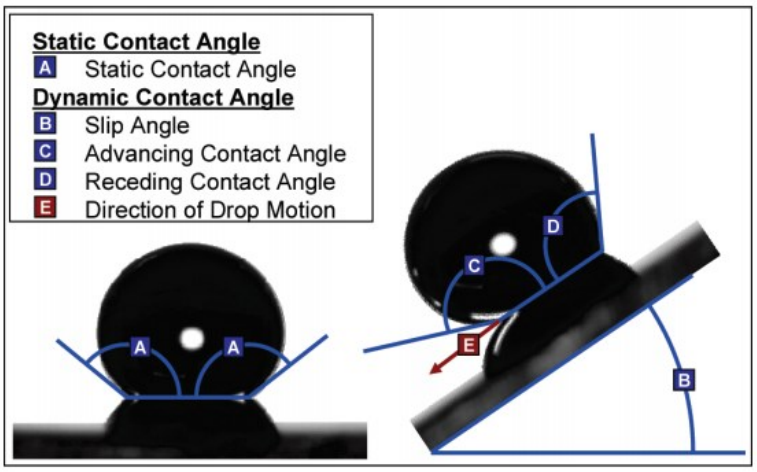

Figure 3.18 Schematics for static and dynamic contact angle (Long et al. 2009)

3.4 Specific Heat Capacity Test

3.4.1 Testing Program

The specific heat capacity test was performed on concrete specimen inside a custom-made calorimetric container. There are control samples and there are two water-to-cement ratios for control samples. Each specimen was tested twice for heat capacity. To minimize the effects of water absorption or crystal growth from re-immersion, the samples were air dried for 24 hours. The test program can be seen in Table 5.

Table 5 Specific heat capacity test program

Type of Test	Water to Cement Ratio	Test Sample	Specimen ID	Number of Test on Each Specimen
Specific Heat Capacity	w/c=0.45	Control concrete cylinder	WC1CON02A	2
			WC1CON03A	2
	w/c=0.43	Control concrete cylinder	WC2CON03A	1
			WC2CON05	1
			WC2CON02B	2

3.4.2 Test Procedure

The standard test method for specific heat capacity is specified in ASTM E1269, "Determining Specific Heat Capacity by Differential Scanning Calorimetry." The summary of the test method per ASTM E1269-11 is: "this test method consists of heating the test material at a controlled rate in a controlled atmosphere through the region of interest. The difference in heat flow into the test material and a reference material or blank due to energy changes in the material is continually monitored and recorded."

The concrete specimens used for the test were made from concrete cylinders of 4 inches diameter and 8 inches height. Most of the test cylinder specimens were the cut cylinders, 6 or 2-inches height and 4 inch diameter. A T-type thermocouple is embedded inside the specimens as shown in the specimen preparation section. A custom-made double insulation setup with foam box (calorimetric container), fiberglass insulation and a smaller container was prepared to test the thermocouple embedded samples. The new calorimetric container setup can be seen in Figure 3.19. T-Type thermocouples are available for measuring temperature in various points of choice.

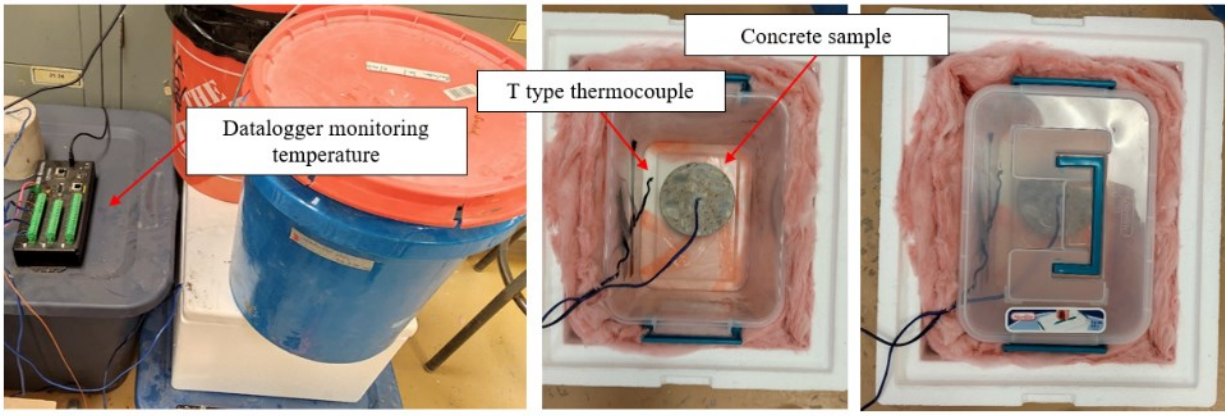

Figure 3.19 New calorimetric container setup for 6-in height cylinder specimens

The testing procedure is illustrated in Figure 3.20. The detailed testing procedure is below:

1. All individual parts are weighted and dried out. The setup is prepared for testing.
2. The dried smaller container inside the foam box includes a thermocouple to record water temperature and the concrete specimen is placed inside of it.
3. The whole system is allowed to reach equilibrium in the lab for 30 minutes.
4. Hot water of 50 °C from water bath is poured inside the smaller container.
5. Immediately the smaller container's cap is closed, top fiberglass insulation is put, and the foam box cap is closed. Two heavy buckets of soil are put on top of the cap to stabilize and minimize the gap in the cap.
6. Depending on the specimen size, around 1-2 hour of data is recorded, the initial reading in water temperature sensor is considered the initial water temperature which may be slightly lower than 50 °C.
7. The highest temperature the concrete specimen will reach during the test is considered the equilibrium temperature. After that the specimen would lose heat and its temperature would reduce.
8. Beyond this temperature both water and concrete start losing temperature.

9. The whole system is weighted after the test to calculate the initial added water weight.
10. All the parts are flushed and dried out for the next test

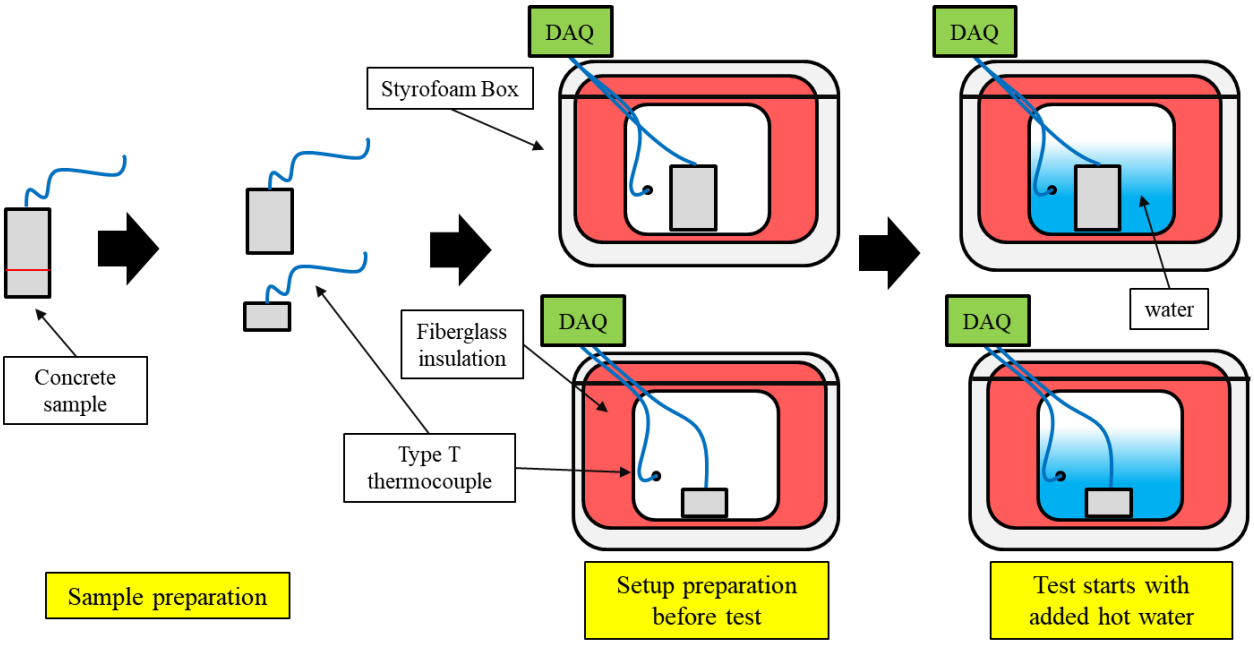

Figure 3.20 Heat capacity test procedure

3.4.3 Sample Test Result

In this section the step-by-step procedure to determine the heat capacity value of each concrete specimen is presented here. As explained in the previous test procedure section, the temperature variations of the concrete specimen and the water, and the room temperature are recorded. One example test is chosen to explain the data processing procedure to calculate the heat capacity. The result of test 10 can be seen in Figure 3.21. Each test would produce a similar graph. Important temperature values that must be extracted from the graph are:

- Equilibrium temperature T_{eq}
- Initial temperatures of water and concrete specimen, respectively ($T_{wi,}T_{ci}$)
- Heat loss value which is determined by a water only test and is assumed to be the same value for samples of the same size as testing condition are fixed.

by using energy balance, we know:

$$Q = mC\Delta T \qquad \textbf{3-1}$$

Q = heat energy (Joules, J)

m = mass of a substance (Kilograms, kg)

C = specific heat (J/kg·K)

Δ is a symbol meaning "the change in"

ΔT = change in Temperature (Kelvins, K)

Heat loss = energy absorbed during test by the calorimetric box (J)

The subscript c refers to concrete, and subscript w refers to water.

Heat absorbed by concrete + Heat absorbed by calorimetric box (heat loss) = Heat loss of the water

$$C_C = \frac{m_w\, C_w \left(T_{wi} - T_{eq}\right) - \text{Heat loss}}{m_c(T_{eq} - T_{ci})} \qquad \textbf{3-2}$$

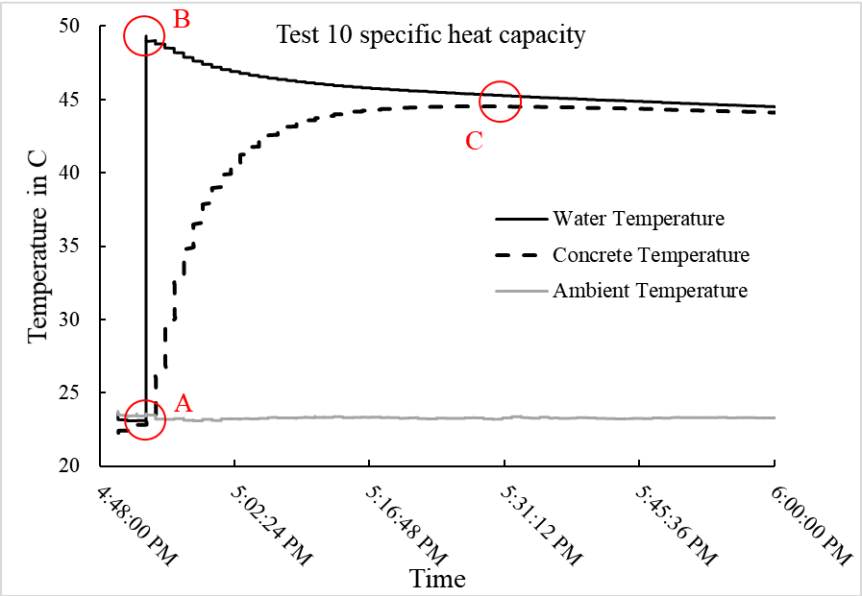

Figure 3.21 Test 10 results of the specific heat capacity test

The heat capacity for test 10 is calculated as follows. The weight of the concrete is $m_c = 2.259$ kg as measured in the lab. The weight of the whole system, meaning water, concrete and the container after the test is 6.375 kg similarly measured after the test in the lab. This value is used to calculate the added water weight.

The weight of the added water can be calculated as $m_w = 2.9798$ kg by knowing that the container's weight which is 1.1362 kg. The initial temperature of concrete specimen T_{ci}, is 22.88 °C as shown in point A in Figure 3.21. This is the temperature the specimen and the container have initially which roughly equals the ambient temperature of the lab. The initial temperature of added water T_{wi} is 49.36 °C as shown in point B in Figure 3.21. This value would be the first reading of the datalogger after adding the hot water to the container and sealing it.

The equilibrium temperature T_{eq}, is 44.5 °C as shown in point C in Figure 3.21. This value is the highest temperature the concrete specimen has experienced as recorded by the datalogger. This can be deduced by the fact that as soon as the concrete is losing heat it is no longer absorbing heat from the water and equilibrium has been reached between the added water and the concrete specimen.

The heat loss value is assumed as 800 J/°C for these tests. This value can be calculated by performing water only tests in the container. To conduct this test, we should perform the test with a material with known specific heat capacity, in this case water. It means instead of using a concrete specimen, we put a specific weight of water inside the calorimetric box and measure its initial temperature. That would replace the concrete initial temperature in the calculations above. After adding the hot water and when the whole system reaches equilibrium, the specific heat capacity of the initial water can be calculated which would not be the same as the value in literature, the "lost heat" can be calculated and implemented in the energy balance formula so that the exact value of the specific heat capacity of water is calculated at the end. This test could also be run on another material, for example a piece of aluminum. By knowing the exact initial temperature, the specific heat capacity of aluminum and its weight, the value of heat loss can be calculated in a similar fashion. In all subsequent and similar tests, this value is assumed to remain constant as the testing conditions are not changed. All the inputs can be seen in Table 6.

Table 6 Test 10 Parameters' description and their values

Parameter	Description	Value	Method of Measurement
m_c	Weight of the concrete specimen	2.259 kg	Direct measurement in lab
m_w	Weight of the added water	2.9798 kg	
T_{ci}	Initial temperature of the concrete specimen	22.88 °C	
T_{wi}	Initial temperature of added water	49.36 °C	
T_{eq}	Equilibrium temperature	44.5 °C	From test result
Heat loss	Energy lost during the test	800 J/°C	From water only test result
C_w	Specific heat capacity of water	4186 J/kg·K	Constant from literature
C_C	Specific heat capacity of concrete specimen	To be calculated	Calculated using energy balance

Using the energy balance formula previously discussed (Eq. **3-2**) we have:

$$C_C = \frac{m_w\, C_w \left(T_{wi} - T_{eq}\right) - 800 \times (T_{eq} - T_{ci})}{m_c(T_{eq} - T_{ci})} \qquad \textbf{3-3}$$

C_w is assumed to be constant and have the value of 4186 J/kg·K (Halliday and Resnick 2013)

$$C_C = \frac{2.9798 \times 4186 \times\ (49.36 - 44.5) - 800 \times (44.5 - 22.88)}{2.259\ \times (44.5 - 22.88)}$$

$$C_C = 887.09 \text{ J/kg·K}$$

This value is within range of previously reported specific heat capacity, which is 750 to 960 J/kg·K (Engineering ToolBox 2003). All other tests would have similar calculations eventually giving out the specific heat capacity of the specimen tested.

3.5 Thermal Conductivity Test

3.5.1 Testing Program

The thermal conductivity of concrete specimen was measured using a thermal analyzer in concrete cylinders with drilled holes for the probe. The details of its measurement method are described in the test procedure section. The test program for thermal conductivity tests can be seen in Table 7. As shown, each specimen has 4 or 2 tests performed on it.

Table 7 Thermal conductivity test program

Type of Test	Water to Cement Ratio	Test Sample	Specimen ID	Number of Tests on Each Specimen
Thermal Conductivity	**w/c=0.45**	Control Concrete Cylinder	WC1CON01A	4
			WC1CON04A	4
	w/c=0.43	Control Concrete Cylinder	WC2CON01A	4
			WC2CON04A	4

3.5.2 Test Procedure

"KD2 Pro Thermal Properties Analyzer" is used for the measurements. RK-1 rock sensor with the description shown in Table 8is the sensor used for the measurements. The KD2 Pro analyzer, the probe, and the thermal paste used for the tests can be seen in Figure 3.22. The method used in the ASTM and IEEE thermal conductivity/resistivity measurement standards (IEEE 442 and ASTM 5334) is generally called the transient line heat source or transient heated needle method. The KD2 Pro complies fully with ASTM D5334-14. Samples are drilled, and the drilled hole is cleaned and dried. Then the holes are filled with thermal paste and tests are performed.

Table 8 RK-1 rock sensor description

Specifications	**Descriptions and values**
Accuracy	± 10% from 0.2 – 6 W/(m.K)
Measurement Speed	10 minutes read time
Range	0.1 o 6 W/(m.K), 17° to 1000° C
Operating Temperature	-50 to 150 °C

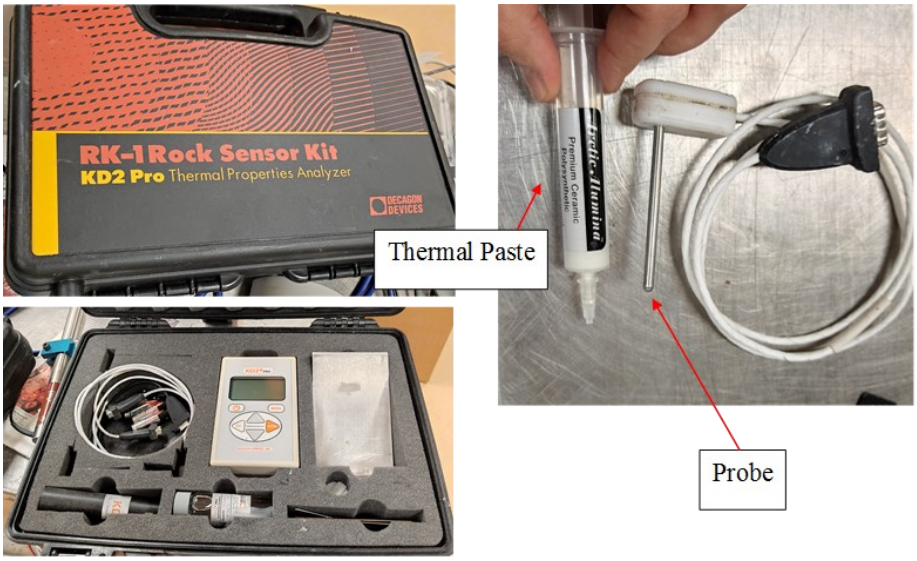

Figure 3.22 "KD2 Pro Thermal Properties Analyzer", Its Probe and thermal paste

Initially as mentioned, specific concrete cylinders are cut in half, have been drilled to the specifications of the sensor's probe, washed and dried. The schematics of the drilling can be seen in Figure 3.23. Figure 3.24 shows some pictures of the preparation steps.

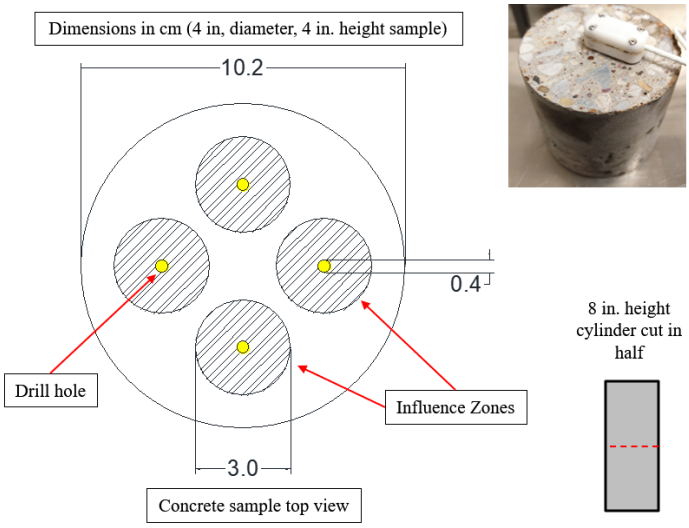

Figure 3.23 Schematics of the drilling plan for concrete cylinders for thermal conductivity tests

Figure 3.24 Pictures of specimen preparation steps

The dried specimen would then be tested using the KD2 and the RK-1 probe. A typical testing setup would look like Figure 3.25.

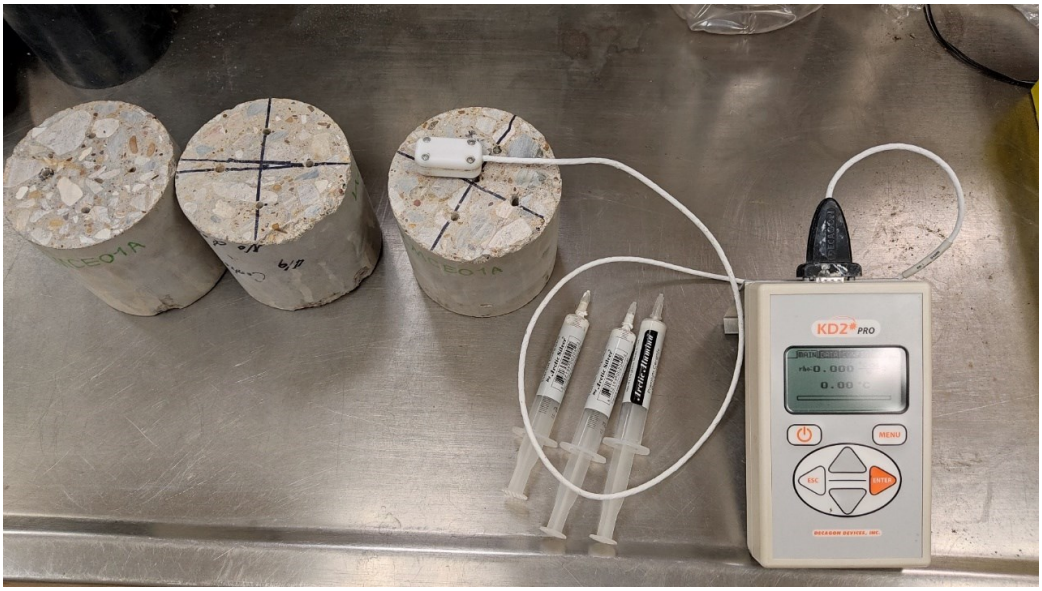

Figure 3.25 Thermal conductivity test ready to start

3.5.3 Sample Test Result

The KD2 would give out a result as shown in Table 9. This would include the initial or ambient temperature, the thermal conductivity which is the goal of the test and error values.

Table 9. Sample thermal conductivity test result

Sample ID	Thermal Resistivity rho (C.cm/W)	Thermal conductivity K (W/m.K)	Initial temperature (°C)	Error value
WC1CON01A	41.76	2.395	22.93	0.0032

It should be noted that the KD2 in rock or concrete would repeat the readings and the measurements several times hence the longer testing time required for such samples and then would compare the variance between the results. If the error value is greater than 0.001, the test result is not reliable, and the test must be repeated. This can be confirmed for all the tests performed for this property as shown in detail in appendix A.

Chapter 4 Results And Discussion

4.1 Introduction

In this chapter, after understanding the test procedures and the testing programs, the final results of the various tests discussed are provided and discussed. Ice adhesion tests are the main focus of this study but contact angle measurements, specific heat capacity and thermal conductivity tests were also performed to support or help better understand the adhesion test results.

4.2 Ice Adhesion Test

In this section, all test results are presented. The more detailed results of the ice adhesion tests can be accessed through appendix A. The raw test data is also provided with the Study. The results of the ice adhesion shear tests can be seen in Figure 4.1 and Figure 4.2.

The results show a clear performance of the PAVIX surface treatment on the reduction of ice adhesion values. PAVIX-treated specimens show up to about 97% reduction in ice adhesion. This is true despite the rough surface effects of the PAVIX treated samples versus the smooth cut surfaces of the control samples. As the higher roughness increases the shear stress it can be concluded that the actual reduction achieved by PAVIX is expected to be higher than the measured percentage (97%). A summary of the test results can be seen in Table 10 and Table 11.

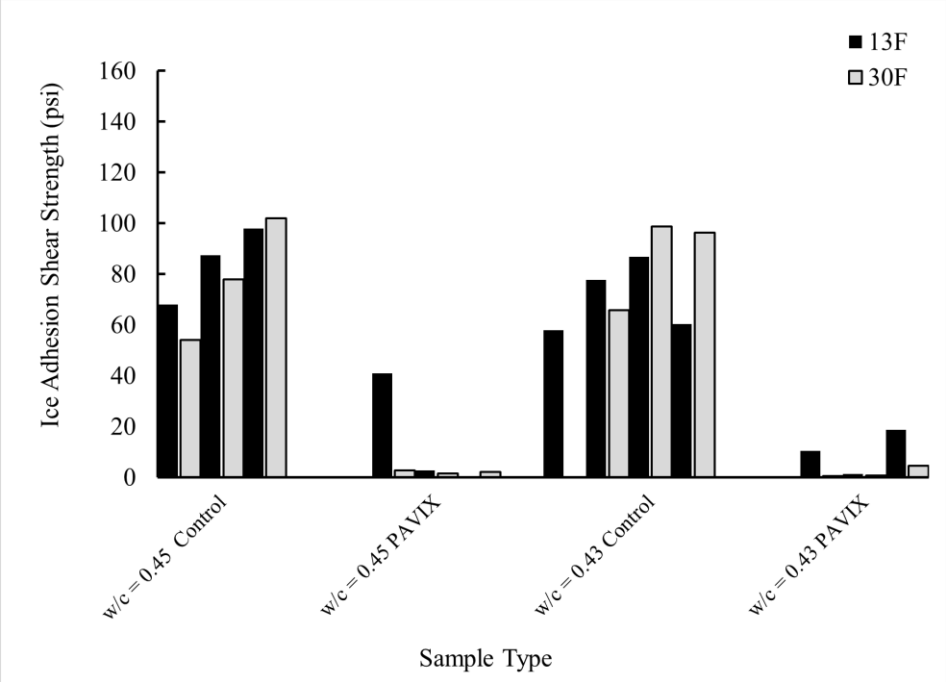

Figure 4.1 Ice adhesion test all results

An in-depth investigation of the mechanisms that contribute to this adhesion reduction is needed to better understand this phenomenon. The hydrophobicity of the surface as a direct result of PAVIX treatment would be the prominent factor as hydrophobicity has been reported previously on ice adhesion reduction on metallic surfaces various times (Bascom et al. 1969; Bharathidasan et al. 2014).

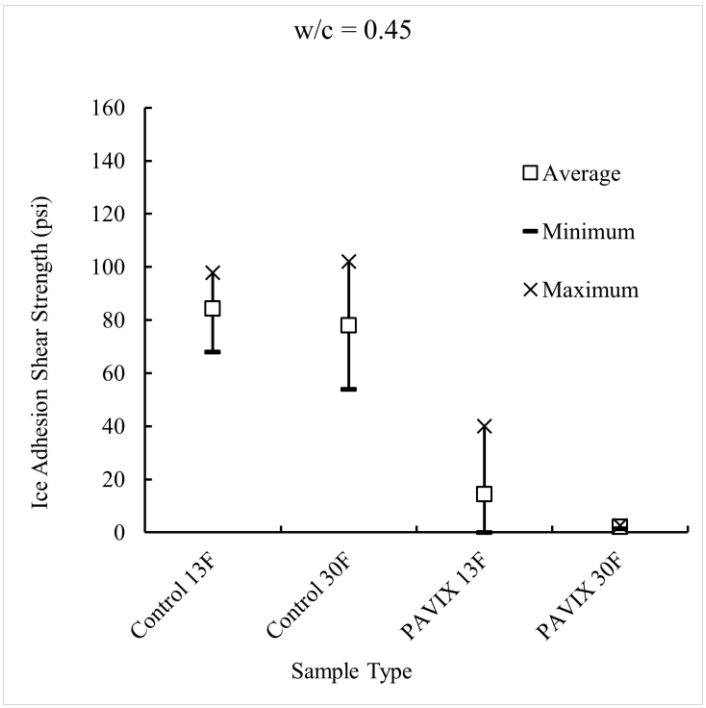

(a)

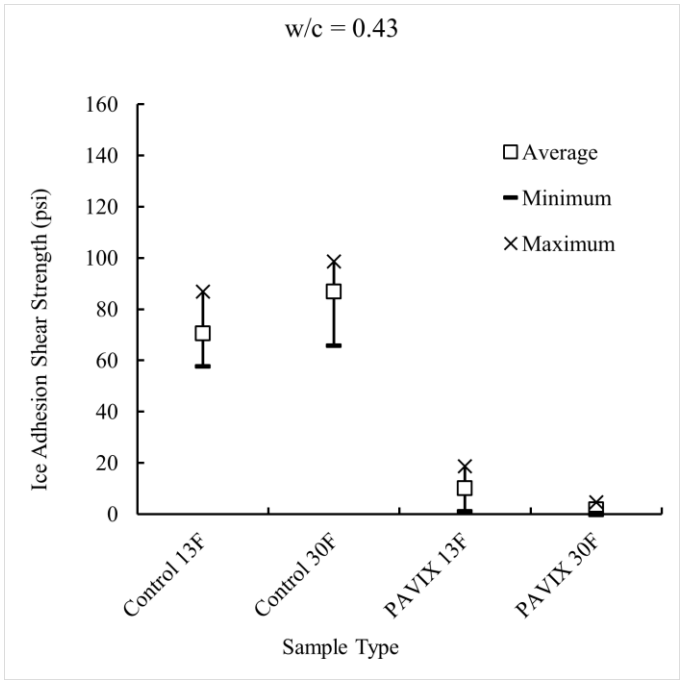

(b)

Figure 4.2 Ice adhesion of specimens – sample variance: (a) w/c 0.45, (b) w/c 0.43

Table 10 Ice adhesion test results summary for w/c = 0.45

Water Cement Ratio	Test Condition	Sample Type	Adhesion of Ice to Concrete Surface (psi)			Standard Deviation (S.D.)	Change
			Average	Minimum	Maximum		
w/c = 0.45	13 F	Control	84.4	68	97.8	14.9	-
		PAVIX	14.46	0*	40	20.25	**-82.8%**
	30 F	Control	77.93	54	102	24	-
		PAVIX	2	1.4	2.7	0.65	**-97.4%**

* The ice-disc was separated from the concrete disc before shearing.

Table 11 Ice adhesion test result summary for w/c = 0.43

Water Cement Ratio	Test Condition	Sample Type	Adhesion of Ice to Concrete Surface (psi)			Standard Deviation (S.D.)	Change
			Average	Minimum	Maximum		
w/c = 0.43	13 F	Control	70.6	57.8	86	14.53	-
		PAVIX	10.1	1.2	18.7	8.7	**-85.6%**
	30 F	Control	86.9	65.8	98.6	16.6	-
		PAVIX	1.9	0.5	4.5	2	**-97.8%**

4.3 Contact Angle

The summary of contact angles of concrete surfaces is tabulated in Table 12 with various water-cement ratios and treatments. The contact angle of the control sample with w/c=0.43 is around 56.6º, meaning that the surface is hydrophilic, as shown in Figure 4.3. The static contact angle for the control sample with w/c=0.45 was difficult to measure since the specimen surface has a bunch of small cracks. When a water droplet was put on the surface, water was quickly dissipated by those cracks. The static contact angles of top treated specimens with w/c=0.45 and w/c=0.43 are 104.7º and 98.1º as shown in Figure 4.4. The results illustrated that after applying PAVIX CCC100 on concrete block surface, the surface becomes hydrophobic, as confirmed by having the contact angle of the treated surface above 90º. In addition, the water-cement ratio has less effect on specimen surface wettability.

Table 12 Summary of contact angles for all specimens (Hashemi Senejani, Lei, Yu 2022)

Test ID	Specimen	Water cement ratio (w/c)	Contact angle (°)	
			Static	Advancing/receding
1	Control	0.45	-	-
2	Top treated		104.7	92.2/47.7
3	Control	0.43	56.6	-
4	Top treated		98.1	100.3/40.8

(a) (b)

Figure 4.3 Contact angle measurement for control samples: (a) w/c=0.45, (b)w/c=0.43

(a) (b)

Figure 4.4 Contact angle measurement for top treated samples: (a) w/c=0.45, (b)w/c=0.43 (Hashemi Senejani, Lei, Yu 2022)

In addition to static contact angle measurement, dynamic contact angle measurements for top treated samples were also conducted. Figure 4.5 presents the advancing and receding contact angles for treated samples. Ideally, a perfectly homogeneous surface has a theoretical contact angle hysteresis of 0°. The hysteresis here means the difference between advancing and receding contact angles. However, in this study average contact angle hysteresis is 52°. This large hysteresis indicates a chemical heterogeneity on the concrete surface after applying PAVIX CCC 100.

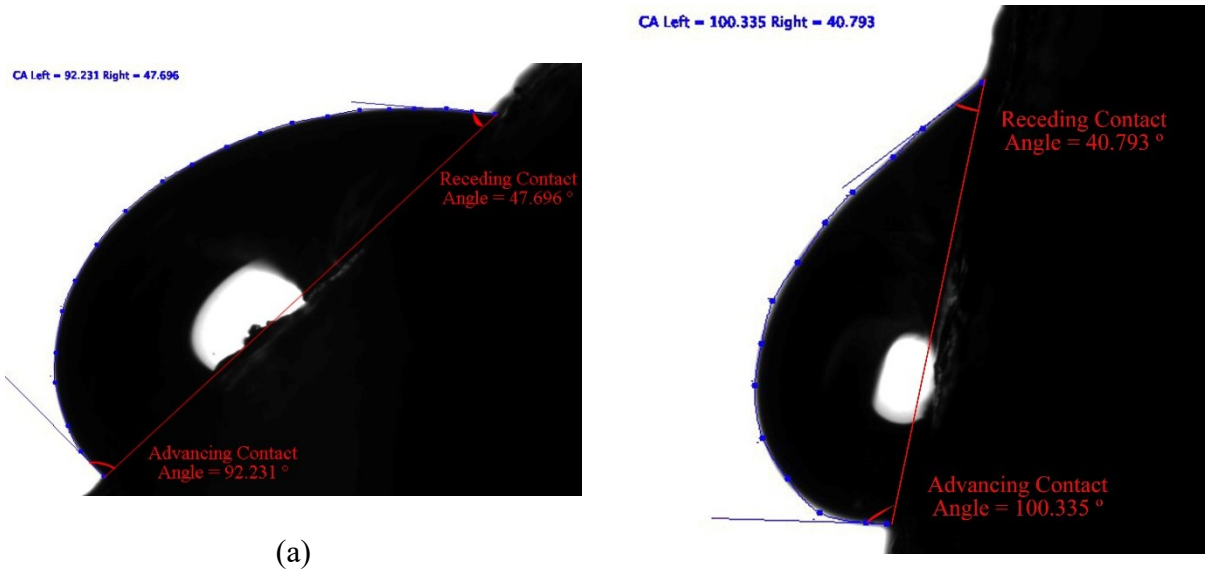

(a) (b)

Figure 4.5 Dynamic contact angle measurement for treated samples: (a) w/c=0.45, (b)w/c=0.43 (Hashemi Senejani, Lei, Yu 2022)

4.4 Specific Heat Capacity

The results of the specific heat capacity tests can be seen in Figure 4.6. A summary of the results can be seen in Table 13. The specific heat capacity results do have a high variance but are well within reported range for concrete specific heat capacity in the literature which is a range from about 750 J/kg.C to 1200 J/kg.C. Please note that as further pilot tests were being performed on samples of experimental mixtures and their results are not included, the specific heat capacity results here cannot be used in the interpretation of the ice adhesion test results yet.

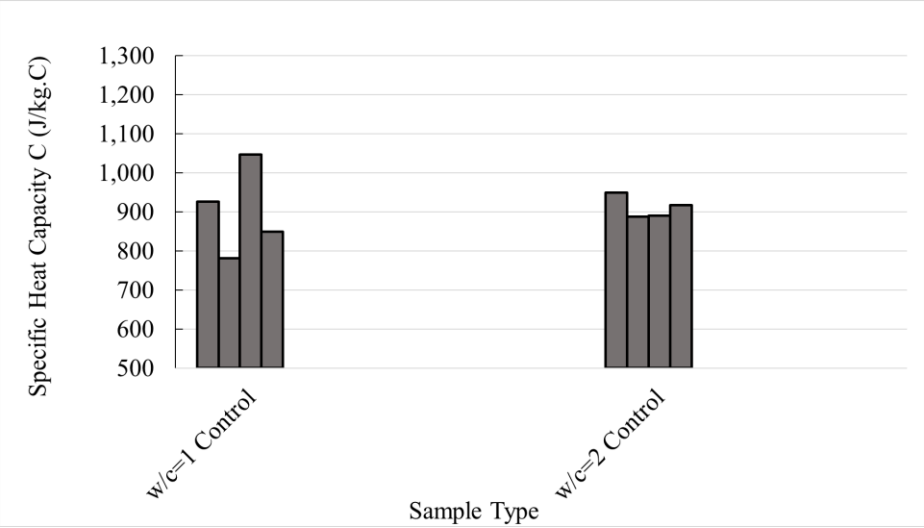

(a)

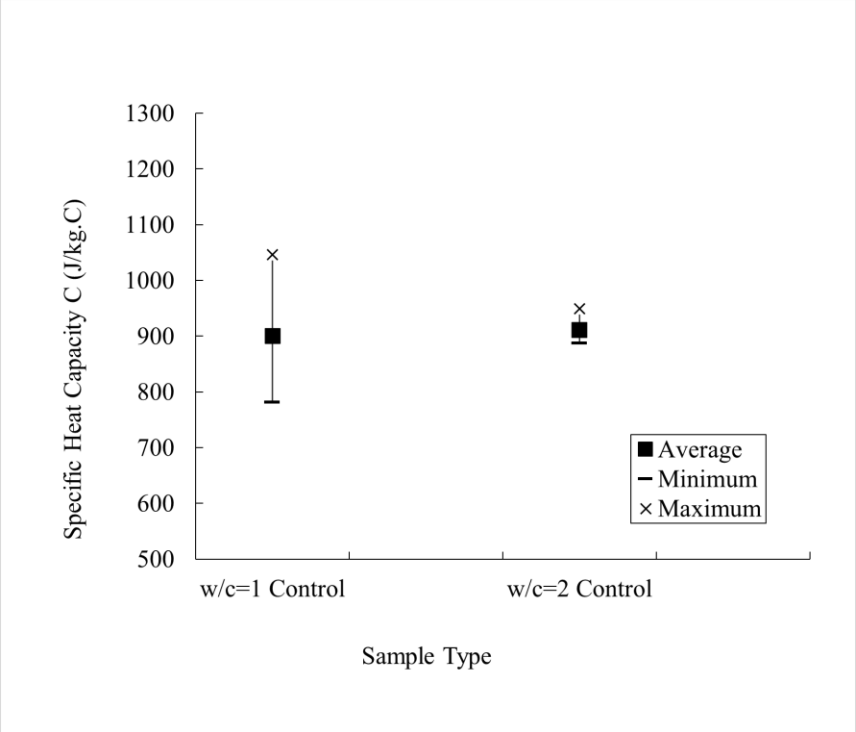

(b)

Figure 4.6 Specific heat capacity results, (a) bar chart, (b) sample variance

Table 13 Summary of specific heat capacity test results

Water Cement Ratio	Sample Type	Specific Heat Capacity C (J/kg.C)			Standard Deviation (SD)	Increase
		Ave.	Min.	Max.		
w/c=0.45	Control	900.359	781.393	1046.051	113.571	-
w/c=0.43	Control	910.952	887.086	949.326	28.812	

4.5 Thermal Conductivity

The results of the thermal conductivity tests can be seen in Figure 4.7. Each concrete type has either six or eight measurements which are from two specimens cut from two different cylinders. The higher cement content shows a slight reduction in thermal conductivity as well. The summary of the results is shown in Table 14. Thermal conductivity of the two control concrete, w/c 0.45 and 0.43, is almost the same (less than 3% difference). Please note that as further pilot tests were being performed on samples of experimental mixtures and their results are not included, the thermal conductivity results here cannot be used in the interpretation of the ice adhesion test results yet.

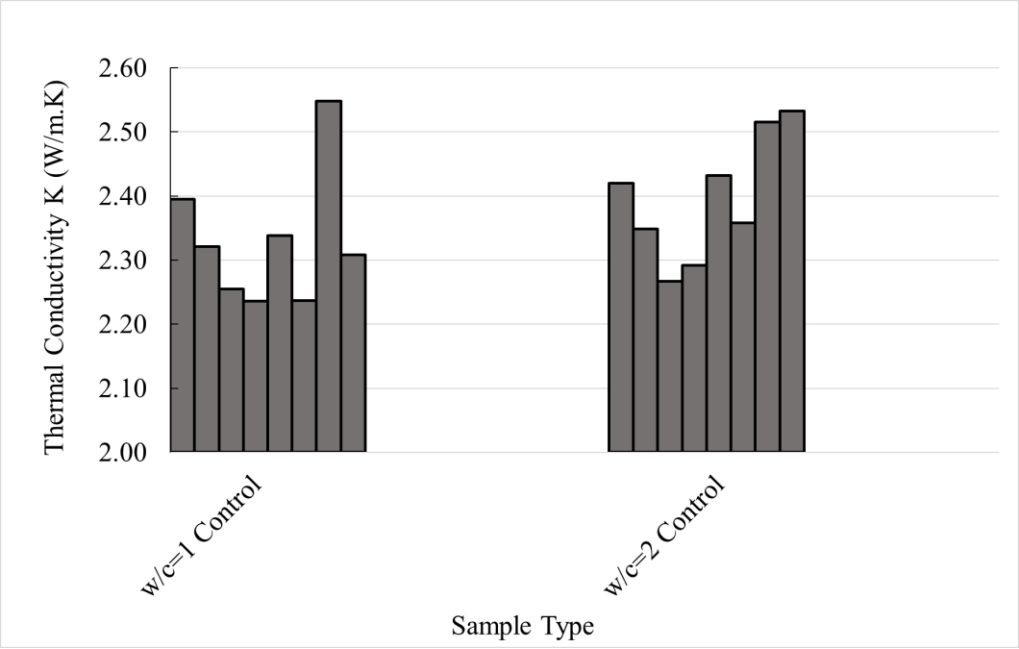

(a)

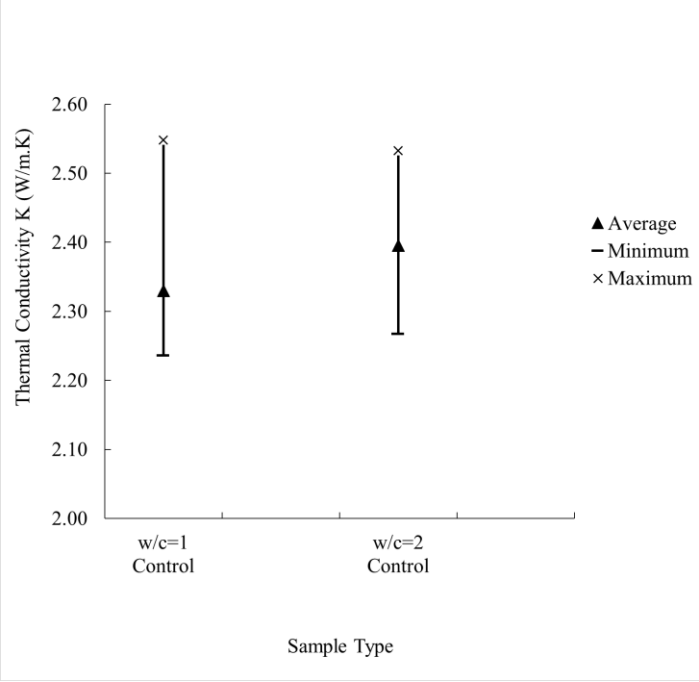

(b)

Figure 4.7 Thermal conductivity test results: (a) bar chart, (b) average values with sample variance

Table 14 Summary of thermal conductivity test results

Water to Cement Ratio	Sample Type	Thermal conductivity K (W/m.K)			Standard Deviation (SD)	Increase
		Average	Minimum	Maximum		
w/c=0.45	Control	2.330	2.236	2.548	0.104	-
w/c=0.43	Control	2.396	2.267	2.533	0.097	-

Chapter 5 Summary And Conclusions

5.1 Summary

This study described the series of tests run to analyze the performance of the Chem-Crete PAVIX CCC100 waterproofing material on concrete regarding ice adhesion at two water-to-cement ratios of 0.45 and 0.43 and ice forming temperatures of 30 ^{o}F and 13 ^{o}F. The conclusions are drawn from the test results as follows.

5.2 Conclusions

These are conclusions from the direct shear tests performed on topically treated and untreated concrete disks:

1. The ice-concrete adhesion for the two control concrete mixes at 30 ^{o}F and 13 ^{o}F is around 80 psi.
2. PAVIX surface-treated specimens show more than 83% reduction in ice adhesion compared to the control specimens. The reduction is consistent for the two concrete mixes.
3. The ice-adhesion reduction increases with the increase of temperature. The ice-adhesion reduction is more than 97% at 30 ^{o}F.

These findings are also correlated to the observed hydrophobicity of the PAVIX treated concrete as summarized below from contact angle measurements:

1. Concrete specimens with two water-cement ratios (0.45 and 0.43) with and without PAVIX treatment were tested for contact angle.
2. Control specimens have hydrophilic surfaces with a contact angle of less than 90°.
3. Concrete specimens with surface-treated PAVIX CCC100 showed a good hydrophobic treated-surface with contact angles significantly greater than 90°.

4. Water cement ratio has a minor effect on concrete surface wettability.
5. Larger hysteresis was found for dynamic contact angle, meaning that a heterogeneous chemical layer was formed after applying PAVIX CCC100.

5.3 Limitations and Recommendations

The reported results although very promising in the performance of the material are needed to be interpreted carefully as the custom testing methods used are not standardized yet and the procedures included could have increased measurements, considerations, and repeatability. The tests were the first of many in the future to further investigate this phenomenon. The author suggests the modification of adhesion tests to become more streamlined so the number of tests performed can increase greatly. This would reduce the effects of variance that is inherent when dealing with concrete mixtures that are not homogeneous entities. Also the fluctuation of natural ambient temperature, the quality of the ice being prepared, and its formation can create various results. The following suggestions are considered for the continuation of this work:

- A clear rationale for the w/c (water to cement ratio) selection must be provided and larger values of w/c can be chosen, and their performance can be compared.
- An important aspect of the performance of the PAVIX material must be the durability as it is subject to severe abrasion due to the passage of vehicles and weathering. Pavement specific tests to measure the durability of the material and the degradation of its performance due to abrasion must be conducted.
- An important compromise the PAVIX material can have may be the reduction in friction of the surface in regard to wheels of vehicles, the stoppage time and force, etc. Tests must be conducted to measure the change in friction, and it must be determined whether this would be allowable and acceptable with pavement standards.

- A specific method to prepare ice by letting heat exchange from one direction during ice formation is a possible solution which has been briefly practiced in the past. This method of ice preparation would mitigate the flaws and the variance in the structure of the ice which can have big impacts of the mechanical performance of the ice.
- A dedicated shearing machine installed inside a temperature control room would streamline the testing procedure and a second dedicated temperature control freezer used only for sample preparation would allow for an increased number of tests run in a shorter period of time.
- The addition of various vertical loads to the direct shear test would be beneficial in a few ways, including a better understanding of the shearing performance of the interface and helping a more dictated shearing plane.
- A detailed measurement of the surface roughness of the concrete specimen for each specimen tested allows for a better understanding of the performance.
- Additional tests for ice only, concrete only specimen can also provide additional information regarding the phenomenon.

Overall, being an interesting line of investigation to mitigate the negative effects of ice formation on pavement, the continuation of the research can lead to better understanding the phenomenon and exploring an established method for ice bonding reduction to concrete.

References

Al-Jabari. 2022. *Integral Waterproofing of Concrete Structures: Advanced Protection Technologies of Concrete by Pore Blocking and Lining*.

Al-Rashed, R., and M. Jabari. 2020. "Dual-crystallization waterproofing technology for topical treatment of concrete." *Case Studies in Construction Materials*, 13: e00408. https://doi.org/10.1016/j.cscm.2020.e00408.

B. C. Gerwick, and Jr. And D. Berner. 1988. "Thermal and Durability Considerations for Composite Steel/Concrete Sandwich Structures." *SP*, 109: 73–84. https://doi.org/10.14359/2804.

Barker, A., S. Bruneau, and B. Colbourne. 2021. "Bulk Adhesion of Ice to Concrete: Review of Test Programs." *J. Cold Reg. Eng.*, 35(3): 3121001.

Chen, H., Y. Wu, H. Xia, B. Jing, and Q. Zhang. 2018a. "Review of ice-pavement adhesion study and development of hydrophobic surface in pavement deicing." *Journal of Traffic and Transportation Engineering (English Edition)*, 5(3): 224–238.

Chen, H., Y. Wu, H. Xia, B. Jing, and Q. Zhang. 2018b. "Review of ice-pavement adhesion study and development of hydrophobic surface in pavement deicing." *Journal of Traffic and Transportation Engineering (English Edition)*, 5(3): 224–238. https://doi.org/10.1016/j.jtte.2018.03.002.

Fay, L., and X. Shi. 2012. "Environmental Impacts of Chemicals for Snow and Ice Control: State of the Knowledge." *Water Air Soil Pollut*, 223(5): 2751–2770. https://doi.org/10.1007/s11270-011-1064-6.

Fortin, G., and J. Perron. 2012. "Ice Adhesion Models to Predict Shear Stress at Shedding." *Journal of Adhesion Science and Technology*, 26(4-5): 523–553. https://doi.org/10.1163/016942411X574835.

Greaker, N. S. 2014. *Laboratory Measurements of Ice-Concrete Abrasion with Different Types of Ice Quality,* Institutt for bygg, anlegg og transport.

Gustafson. 1982. "Icing conditions on different pavement structures." *Transportation Research Record*, 860: 21.

Hashemi Senejani, H., O. Ghasemi-Fare, D. Yazdani Cherati, and F. Jafarzadeh. 2020. "Investigation of thermo-mechanical response of a geothermal pile through a small-scale physical modelling." *E3S Web Conf.*, 205: 5016. https://doi.org/10.1051/e3sconf/202020505016.

Hashemi Senejani, Lei, Yu. 2022. *Adhesion of Ice to Concrete Surface Treated with PAVIX - Report for Chem-Crete Co*, The University of Texas at Arlington.

Hejazi, V., K. Sobolev, and M. Nosonovsky. 2013. "From superhydrophobicity to icephobicity: forces and interaction analysis." *Sci Rep*, 3(1): 2194. https://doi.org/10.1038/srep02194.

Huang, W., Z. Li, H. Han, and Q. Jia. 2017. "Limit resistive forces from ice frozen to concrete-revetment interface of an inclined dam wall." *Cold Regions Science and Technology*, 141: 181–187. https://doi.org/10.1016/j.coldregions.2017.06.012.

Huovinen S. 1990. *Abrasion of concrete by ice in arctic sea structures*.

Itoh Y. 1988. *Proc., 7th Int. Conf. on Port and Ocean Engineering under Arctic Conditions: Itoh, Y., A. Yoshida, Y. Asai, K. Sasaki, and H. Saeki. 1988. "Testing methods on sea ice-concrete sliding abrasion." In Vol. 3 of Proc., 7th Int. Conf. on Port and Ocean Engineering*

under Arctic Conditions, edited by W. M. Sackinger and M. O. Jeffries, 89–96. Fairbanks, AK: Univ. of Alaska Fairbanks, Geophysical Institute.

Jacobsen, S., G. W. Scherer, and E. M. Schulson. 2015. "Concrete–ice abrasion mechanics." *Cement and Concrete Research*, 73: 79–95. https://doi.org/10.1016/j.cemconres.2015.01.001.

Javan-Mashmool, M., C. Volat, and M. Farzaneh. 2006. "A new method for measuring ice adhesion strength at an ice–substrate interface." *Hydrological Processes*, 20(4): 645–655. https://doi.org/10.1002/hyp.6110.

Jia, Q., W. Tian, Y. C. Lu, X. M. Peng, and J. R. Yu. 2011. "Experimental Study on Adhesion Strength of Freshwater Ice Frozen to Concrete Slab." *Advanced Materials Research*, 243-249: 4587–4591. https://doi.org/10.4028/www.scientific.net/AMR.243-249.4587.

Joshaghani, A., A. A. Ramezanianpour, and M. Jaberizadeh. 2014. "Mechanical Characteristic of Pervious Concrete Considering the Gradation and Size of Coarse Aggregates." *RJEES*, 6(8): 437–442. https://doi.org/10.19026/rjees.6.5255.

Kasaai M. R. 2004. *23rd International Conference on Offshore Mechanics and Arctic Engineering*.

Kreder, M. J., J. Alvarenga, P. Kim, and J. Aizenberg. 2016. "Design of anti-icing surfaces: smooth, textured or slippery?" *Nat Rev Mater*, 1(1). https://doi.org/10.1038/natrevmats.2015.3.

Lv, J., Y. Song, L. Jiang, and J. Wang. 2014. "Bio-inspired strategies for anti-icing." *ACS Nano*, 8(4): 3152–3169. https://doi.org/10.1021/nn406522n.

Ma. 2014. "Research on asphalt concrete pavement deicing technology." *Journal of Southeast University (English Edition)*, 30(3): 336.

Makkonen, L. 1998. "Modeling power line icing in freezing precipitation." *Atmospheric Research*, 46(1-2): 131–142. https://doi.org/10.1016/s0169-8095(97)00056-2.

Makkonen, L. 2012. "Ice Adhesion —Theory, Measurements and Countermeasures." *Journal of Adhesion Science and Technology*, 26(4-5): 413–445. https://doi.org/10.1163/016942411X574583.

Makkonen, L., T. Laakso, M. Marjaniemi, and K. J. Finstad. 2001. "Modelling and Prevention of Ice Accretion on Wind Turbines." *Wind Engineering*, 25(1): 3–21. https://doi.org/10.1260/0309524011495791.

Mittal, K. 2012. "Editorial Note." *Journal of Adhesion Science and Technology*, 26(4-5): 405–406. https://doi.org/10.1163/156856111X619325.

Palacios, A. M., J. L. Palacios, and L. Sánchez. 2012. "Eliciting a human understandable model of ice adhesion strength for rotor blade leading edge materials from uncertain experimental data." *Expert Systems with Applications*, 39(11): 10212–10225. https://doi.org/10.1016/j.eswa.2012.02.155.

Petrenko V. F. 2006. *Physics of ice*.

Pramanik, T. 2021. *An experimental investigation of ice-concrete adhesion and corresponding abrasion,* Memorial University of Newfoundland.

Rønneberg, S., C. Laforte, C. Volat, J. He, and Z. Zhang. 2019. "The effect of ice type on ice adhesion." *AIP Advances*, 9(5): 55304. https://doi.org/10.1063/1.5086242.

Saeki, H., T. Ono, N. E. Zong, and N. Nakazawa. 1985. "Experimental Study on Direct Shear Strength of Sea Ice." *A. Glaciology.*, 6: 218–221. https://doi.org/10.1017/s0260305500010399.

Saeki H. 2010. "Mechanical properties between ice and various materials used in hydraulic structures: The Jin S. Chung Award Lecture, 2010: Saeki, H. 2010. “Mechanical properties between ice and various materials used in hydraulic structures: The Jin S. Chung Award Lecture, 2010.” Int. J. Offshore Polar Eng. 21 (2): 81–90." *Int. J. Offshore Polar Eng.*, 21(2): 81.

Sanchez, F., and K. Sobolev. 2010. "Nanotechnology in concrete – A review." *Construction and Building Materials*, 24(11): 2060–2071. https://doi.org/10.1016/j.conbuildmat.2010.03.014.

Schulz, M., and M. Sinapius. 2015. *Evaluation of different ice adhesion tests for mechanical deicing systems*.

Shi, X., Y. Liu, M. Mooney, M. Berry, B. Hubbard, L. Fay, and A. B. Leonard. 2010. *Effect of chloride-based deicers on reinforced concrete structures*.

Sobolev, K. 2016. "Modern developments related to nanotechnology and nanoengineering of concrete." *Frontiers of Structural and Civil Engineering*, 10(2): 131–141. https://doi.org/10.1007/s11709-016-0343-0.

Sobolev, K., M. Nosonovsky, T. Krupenkin, I. Flores-Vivian, S. Rao, M. Kozhukhova, V. Hejazi, S. Muzenski, B. Bosch, R. Rivero, and National Center for Freight and Infrastructure Research and Education. 2013. *Anti-icing and de-icing superhydrophobic concrete to improve the safety on critical elements on roadway pavements* <https://rosap.ntl.bts.gov/view/dot/26834>.

Tijsen, J., S. Bruneau, and B. Colbourne. 2015. "Laboratory Examination of Ice Loads and Effects on Concrete Surfaces from Bi-Axial Collision and Adhesion Events." *Proceedings of the International Conference on Port and Ocean Engineering Under Arctic Conditions*.

Wang, C., W. Zhang, A. Siva, D. Tiea, and K. J. Wynne. 2014. "Laboratory test for ice adhesion strength using commercial instrumentation." *Langmuir*, 30(2): 540–547. https://doi.org/10.1021/la4044254.

Yang, S., Q. Xia, L. Zhu, J. Xue, Q. Wang, and Q. Chen. 2011. "Research on the icephobic properties of fluoropolymer-based materials." *Applied Surface Science*, 257(11): 4956–4962. https://doi.org/10.1016/j.apsusc.2011.01.003.

Yazdani Cherati, D., O. Ghasemi-Fare, and H. Hashemi Senejani. 2020. "Effects of different parameters on transient heat transfer surrounding energy piles in unsaturated soils." *E3S Web Conf.*, 205: 5015. https://doi.org/10.1051/e3sconf/202020505015.

Appendix A – Detailed Test Results

In this appendix the detailed results of all the tests performed are shown. This would include actual direct shear results of all ice adhesion tests performed. This also include all failed or repeated tests which are shown with an empty cell in their respective table.

Table 15 All ice adhesion tests results (w/c=0.45)

For w/c = 0.45			Test Target Temperature Condition	Average Recorded Temperature (°F)		
Test Sample	**Specimen ID**	**Ice Adhesion Shear Strength (psi) [Peak]**		**Room Temp. during Ice Formation**	**Room temp.– during shearing**	**Shear Box temp. during Shearing**
Control Concrete Cylinder	WC1SUR04B	54	30 °F	29.3	21.7	21.6
	WC1SUR05B	77.8		27.8	29.3	22.3
	WC1SUR06B	102		29.5	28.9	30.2
	WC1CON02B	68	13 °F	-	-	-
	WC1SUR01B	87.4		12.9	30.5	33.4
	WC1SUR03B	97.8		13.9	8.6	11.3
Concrete cylinder with Surface Treated by PAVIX	WC1SUR04A	2.7	30 °F	29.3	21.7	21.6
	WC1SUR05A	1.4		27.8	29.3	22.3
	WC1SUR06A	2		29.5	28.9	30.2
	WC1SUR01A	40.4	13 °F	13.6	11.5	14.9
	WC1SUR03A	2.6		13.9	8.6	11.3

Table 16 All ice adhesion tests results (w/c=0.43)

For w/c = 0.43			Test Target Temperature Condition	Average Recorded Temperature (°F)		
Test Sample	**Specimen ID**	**Ice Adhesion Shear Strength (psi) [Peak]**		**Room Temp. during Ice Formation**	**Room temp.– during shearing**	**Shear Box temp. during Shearing**
Control Concrete Cylinder	WC2SUR04B	65.8	30 °F	30.2	15	19.1
	WC2SUR06B	98.6		30.3	13.6	14.8
	WC2SUR05B	96.3		30.3	13.6	14.8
	WC2SUR02B	60.2	13 °F	13.2	29.12	35.5
	WC2CON07A	77.61		13.3	12.8	13.1
	WC2CON06A	86.8		13.3	12.8	13.1
Concrete cylinder with Surface Treated by PAVIX	WC2SUR05A	0.5	30 °F	30.2	15	19.1
	WC2SUR04A	0.7		30.2	15	19.1
	WC2SUR06A	4.58		30.3	13.6	14.8
	WC2SUR01A	10.4	13 °F	-	-	-
	WC2SUR02A	1.2		13.2	29.12	35.5
	WC2SUR03A	18.7		13.3	30.4	30.9

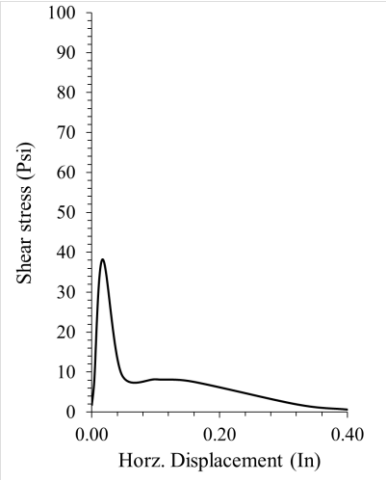

Sample ID

WC2CON03B

w/c = 0.43 Control

Set temp 13 °F

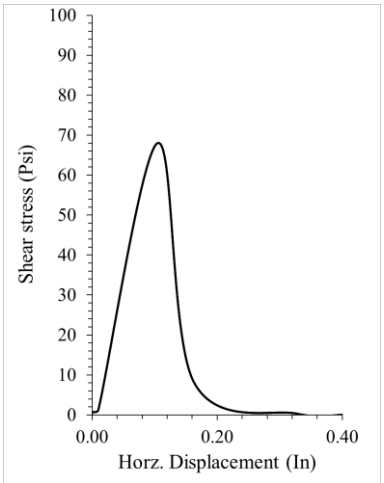

Sample ID

WC1CON02B

w/c = 0.45control

Set temp 13 °F

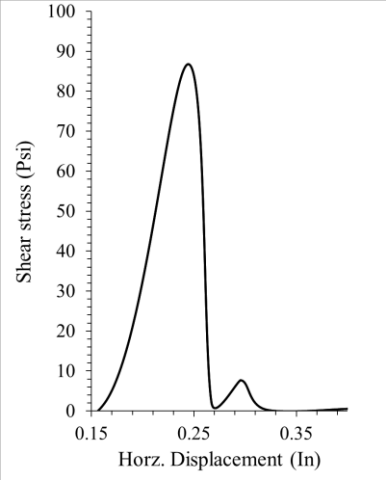

Sample ID

WC2CON04B

w/c = 0.43 control

Set temp 13 °F

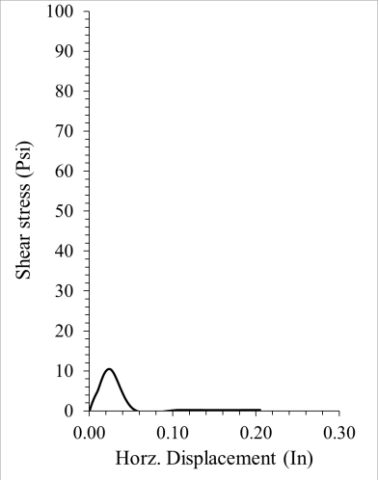

Sample ID

WC2SUR01A

w/c = 0.43 PAVIX surface treated

Set temp 13 °F

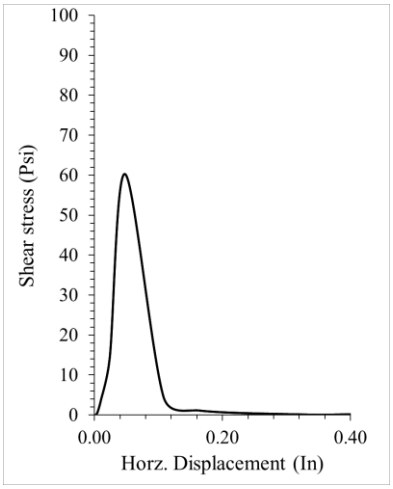

Sample ID
WC2SUR02B
w/c = 0.43 Control
Set temp 13 °F
Measured ave. temp. 13.3 °F

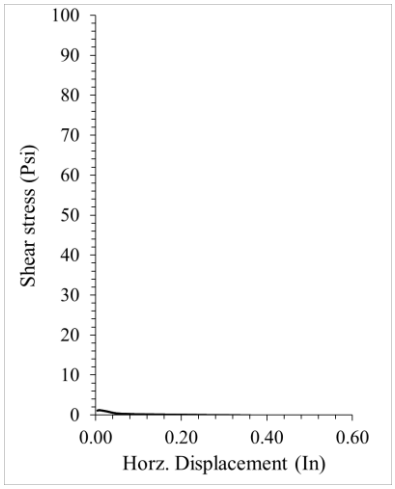

Sample ID
WC2SUR02A
w/c = 0.43 PAVIX surface treated
Set temp 13 °F
Measured ave. temp. 13.2 °F

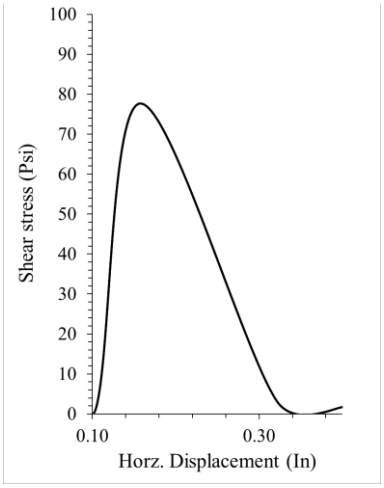

Sample ID
WC2CON06A
w/c = 0.43 Control
Set temp 13 °F
Measured ave. temp. 13.3 °F

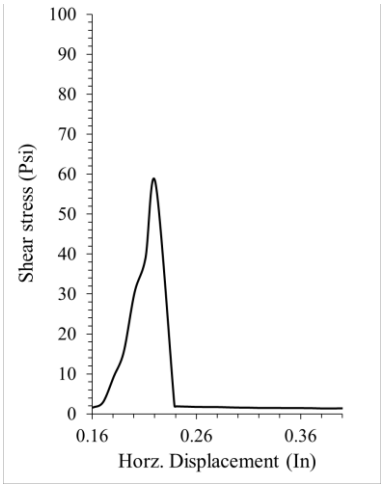

Sample ID
WC2CON07A
w/c = 0.43 Control
Set temp 13 °F
Measured ave. temp. 13.3 °F

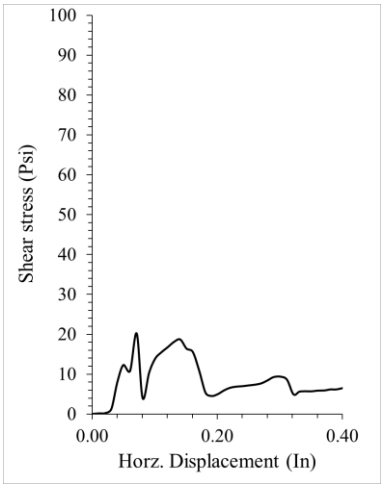

Sample ID
WC2SUR03A
w/c = 0.43 PAVIX surface treated
Set temp 13 °F
Measured ave. temp. 13.3 °F

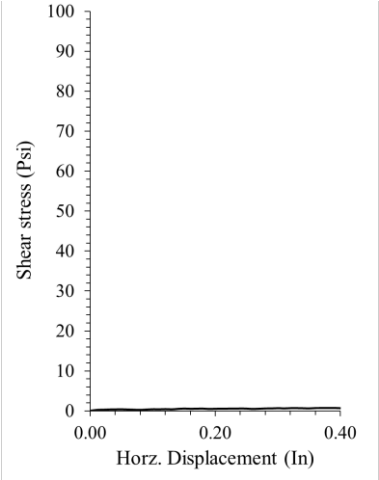

Sample ID
WC2SUR05A
w/c = 0.43 PAVIX surface treated
Set temp 30 °F
Measured ave. temp. 30.2 °F

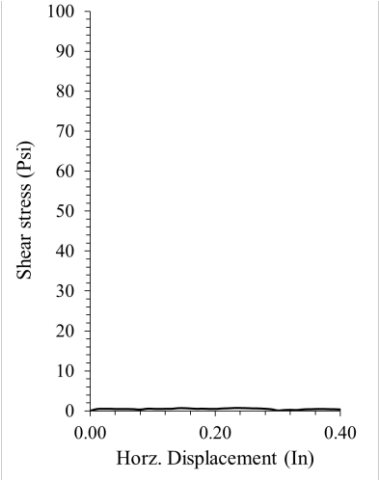

Sample ID
WC2SUR04A
w/c = 0.43 PAVIX surface treated
Set temp 30 °F
Measured ave. temp. 30.2 °F

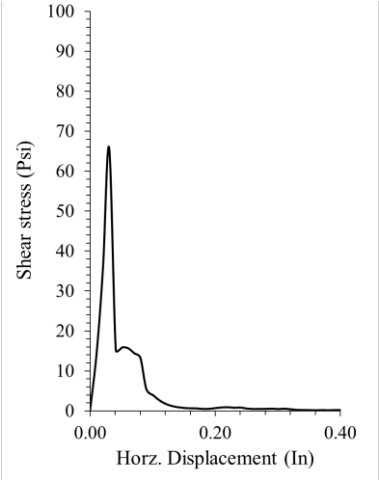

Sample ID
WC2SUR04B
w/c = 0.43 Control

Set temp 30 °F
Measured ave. temp. 30.2 °F

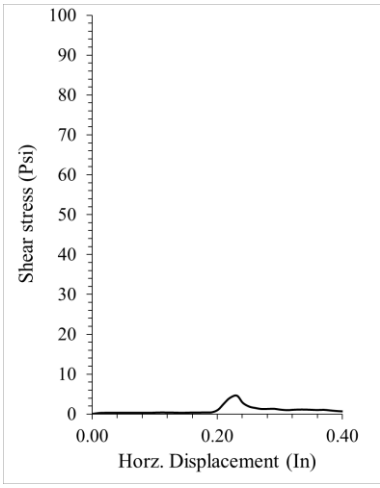

Sample ID
WC2SUR06A
w/c = 0.43 PAVIX surface treated
Set temp 30 °F
Measured ave. temp. 30.3 °F

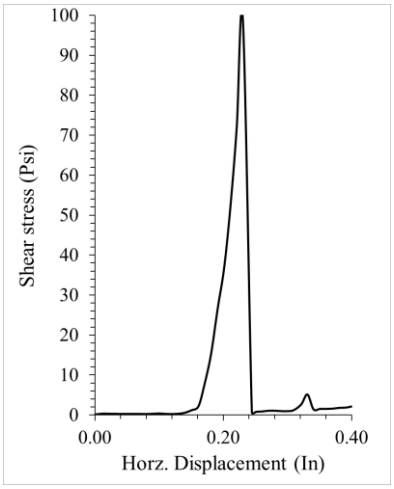

Sample ID
WC2SUR06B
w/c = 0.43 Control

Set temp 30 °F
Measured ave. temp. 30.3 °F

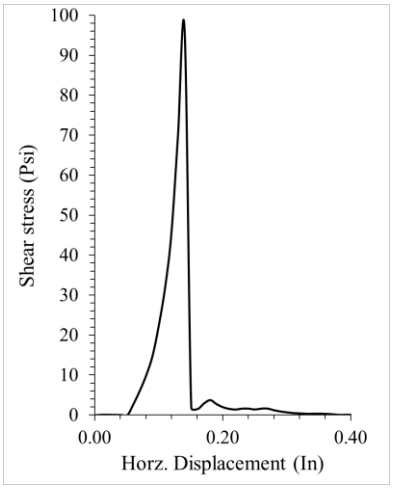

Sample ID
WC2SUR05B
w/c = 0.43 Control

Set temp 30 °F
Measured ave. temp. 30.3 °F

Ice detached before

the test

Ice adhesion ≈ 0 psi

Sample ID
WC1SUR01A
w/c = 0.45 PAVIX surface treated
Set temp 13 °F
Measured ave. temp. 13.6 °F

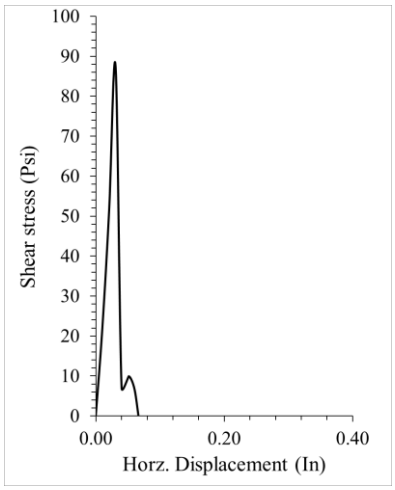

Sample ID
WC1SUR01B
w/c = 0.45 Control
Set temp 13 °F
Measured ave. temp. 13.6 °F

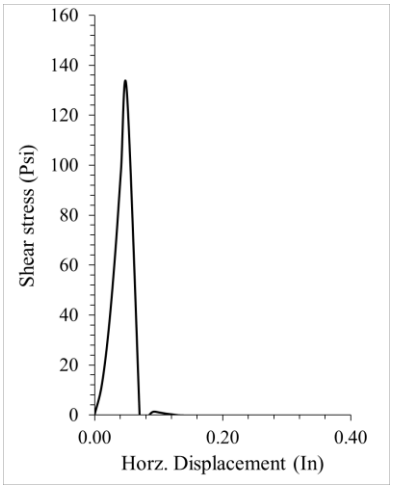

Sample ID
WC1SUR03B
w/c = 0.45 Control
Set temp 13 °F
Measured ave. temp. 13.9 °F

Ice detached before

the test

Ice adhesion ≈ 0 psi

Sample ID
WC1SUR03A
w/c = 0.45 PAVIX
Set temp 13 °F
Measured ave. temp. 13.9 °F

Sample ID
WC1SUR03B
w/c = 0.45 Control
Set temp 13 °F

Sample ID
WC1SUR03A
w/c = 0.45 PAVIX
Set temp 13 °F

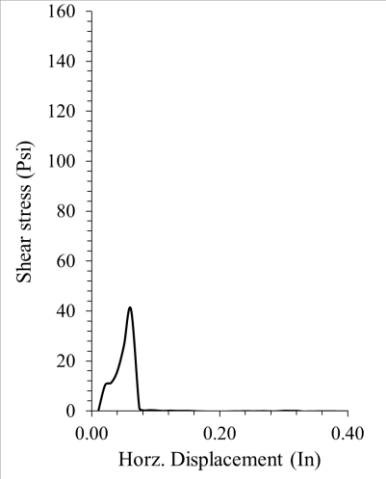

Sample ID
WC1SUR01A
w/c = 0.45 PAVIX
Set temp 13 °F
Measured ave. temp. 13.6 °F

Ice detached before

the test

Ice adhesion ≈ 0 psi

Sample ID
WC1SUR02A
w/c = 0.45 PAVIX
Set temp 13 °F
Measured ave. temp. 13.6 °F

Sample ID
WC1SUR01A
w/c = 0.45 PAVIX
Set temp 13 °F

Sample ID
WC1SUR02A
w/c = 0.45 PAVIX
Set temp 13 °F

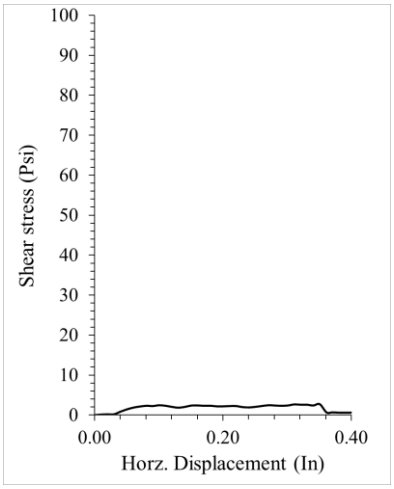

Sample ID
WC1SUR04A
w/c = 0.45 PAVIX
Set temp 30 °F
Measured ave. temp. 29.3 °F

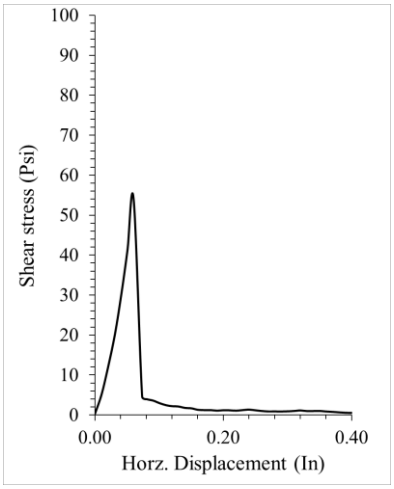

Sample ID
WC1SUR04B
w/c = 0.45 Control
Set temp 30 °F
Measured ave. temp. 29.3 °F

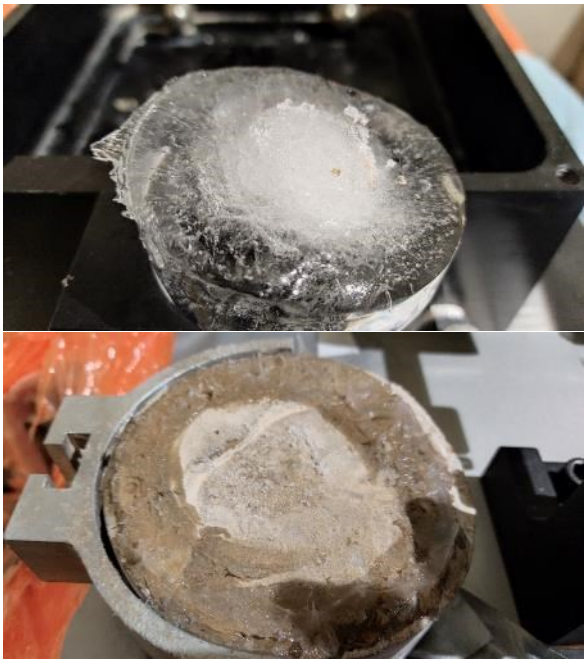

Sample ID
WC1SUR04A
w/c = 0.45 PAVIX
Set temp 30 °F

Sample ID
WC1SUR04B
w/c = 0.45 Control
Set temp 30 °F

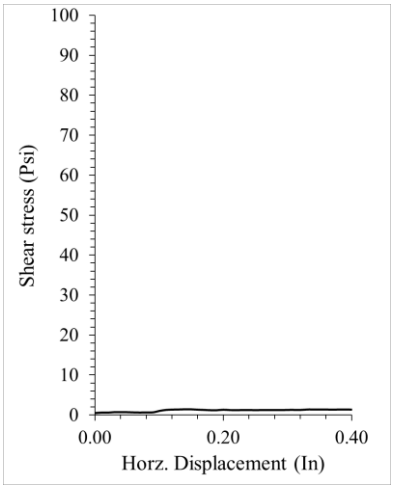

Sample ID
WC1SUR05A
w/c = 0.45 PAVIX
Set temp 30 °F
Measured ave. temp. 27.8 °F

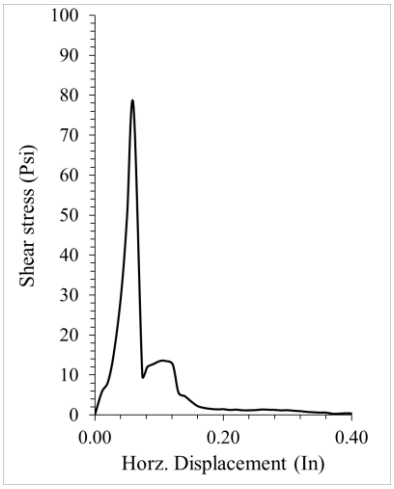

Sample ID
WC1SUR04B
w/c = 0.45 Control
Set temp 30 °F
Measured ave. temp. 27.8 °F

Sample ID
WC1SUR05A
w/c = 0.45 PAVIX
Set temp 30 °F

Sample ID
WC1SUR04B
w/c = 0.45 Control
Set temp 30 °F

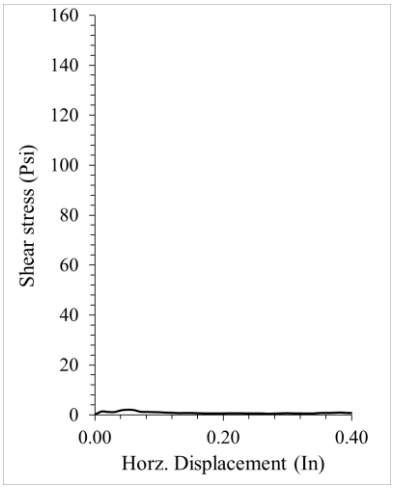

Sample ID
WC1SUR06A
w/c = 0.45 PAVIX
Set temp 30 °F
Measured ave. temp. 29.5 °F

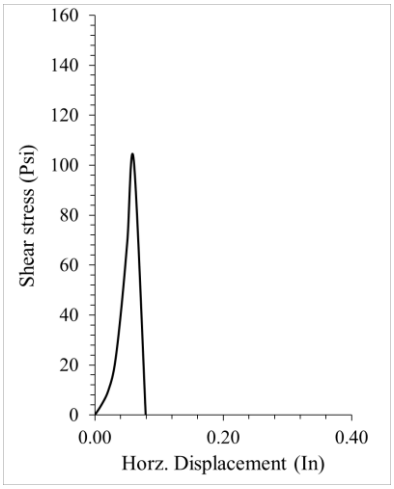

Sample ID
WC1SUR06B
w/c = 0.45 Control
Set temp 30 °F
Measured ave. temp. 29.5 °F

Sample ID
WC1SUR06A
w/c = 0.45 PAVIX
Set temp 30 °F

Sample ID
WC1SUR06B
w/c = 0.45 Control
Set temp 30 °F

Table 17 Specific heat capacity detailed tests results

Temperatures are in °C, weights are in grams (g)						Heat loss considered from container (J/C):800						
Test #	Sample ID	Weight of concrete	Initial water container weight	Initial Temp	added water temp	Whole system weight	added water weight	Delta T initial	Equilibrium temp	Delta T added	MC concrete (J/C)	**C Concrete J/kg.C**
1	WC1CON02A	2770.2	1136.2	19.4	49.0	6650	2743.6	22.9	42.3	6.7	2563.7	**925.4**
2	WC1CON03A	2757.3	1136.2	24.3	48.8	7100	3206.5	20.1	44.3	4.4	2154.5	**781.3**
5	WC2CON03A	2167.4	1036.2	23.1	49.1	6005	2801.4	20.9	44.0	5.1	2057.5	**949.3**
6	WC2CON02B	1013.8	1136.2	21.2	50.1	4250	2100.0	23.2	44.3	5.6	929.4	**916.7**
8	WC1CON02A	2763.6	1136.2	22.3	50.2	7210	3310.2	22.0	44.3	5.8	2890.8	**1046.0**
9	WC1CON03A	2761.1	1136.2	22.7	48.3	6850	2952.7	20.4	43.1	5.2	2342.8	**848.5**
10	WC2CON02A	2259.0	1136.2	22.9	49.3	6375	2979.8	21.6	44.5	4.8	2003.9	**887.0**
14	WC2CON05	3903.0	1136.2	21.8	49.5	7650	2610.8	19.9	41.7	7.7	3476.0	**890.6**

Table 18 Thermal conductivity detailed tests results

Sample ID	Pilot hole #	Test #	Thermal Resistivity rho (C.cm/W)	Thermal conductivity K (W/m.K)	Initial Temperature (°C)	Error value
WC1CON01A	1	1	41.76	2.395	22.93	0.0032
	2	1	43.09	2.321	22.89	0.0017
	3	1	44.35	2.255	22.91	0.0025
		2	44.72	2.236	23.03	0.0031
	4	1	42.78	2.338	22.95	0.0035
WC2CON01A	1	1	41.33	2.42	22.99	0.0023
	2	1	42.58	2.349	23.06	0.003
	3	1	44.11	2.267	23.11	0.0024
		2	43.64	2.292	23.17	0.0032
	4	1	41.13	2.432	23.11	0.0055
WC1CON04A	1	1	44.7	2.237	22.69	0.006
	2	1	39.25	2.548	22.81	0.0049
		2	43.32	2.308	22.96	0.0017
WC2CON04A	1	1	42.42	2.358	23.82	0.0034
	2	1	39.77	2.515	23.78	0.0052
	3	1	48.89	2.045	23.51	0.0091
		2	39.48	2.533	24.12	0.032